NASA TECHNICAL NOTE

NASA TN D-5443

NASA TN D-5443

A FEASIBILITY STUDY OF DETERMINING PHYSICAL PROPERTIES OF THE MARTIAN ATMOSPHERE BY USE OF SOLAR OCCULTATION AS SEEN FROM AN ARTIFICIAL SATELLITE

by H. Andrew Wallio and James R. Williams

Langley Research Center

Langley Station, Hampton, Va.

NATIONAL AERONAUTICS AND SPACE ADMINISTRATION • WASHINGTON, D. C. • OCTOBER 1969

1. Report No. NASA TN D-5443	2. Government Accession No.	3. Recipient's Catalog No.
4. Title and Subtitle A FEASIBILITY STUDY OF DETERMINING PHYSICAL PROPERTIES OF THE MARTIAN ATMOSPHERE BY USE OF SOLAR OCCULTATION AS SEEN FROM AN ARTIFICIAL SATELLITE		5. Report Date October 1969 6. Performing Organization Code
7. Author(s) H. Andrew Wallio and James R. Williams		8. Performing Organization Report No. L-6713
9. Performing Organization Name and Address NASA Langley Research Center Hampton, Va. 23365		10. Work Unit No. 125-17-06-04-23 11. Contract or Grant No.
12. Sponsoring Agency Name and Address National Aeronautics and Space Administration Washington, D.C. 20546		13. Type of Report and Period Covered Technical Note 14. Sponsoring Agency Code

15. Supplementary Notes

16. Abstract

The occultation of sunlight through five model Martian atmospheres as seen from an artificial satellite is examined. The mathematical model of the atmospheres include effects of refraction, Rayleigh scattering, limb darkening, and finite sun size. The study further shows that it is feasible to use the occultation of the sun as a method of determining scale height and surface pressure provided the shorter visible light wavelengths (3500 angstroms) are used.

17. Key Words Suggested by Author(s)	18. Distribution Statement
Martian atmospheres Solar occultation Satellites	Unclassified – Unlimited

19. Security Classif. (of this report)	20. Security Classif. (of this page)	21. No. of Pages	22. Price*
Unclassified	Unclassified	63	$3.00

*For sale by the Clearinghouse for Federal Scientific and Technical Information
Springfield, Virginia 22151

A FEASIBILITY STUDY OF DETERMINING PHYSICAL PROPERTIES OF THE MARTIAN ATMOSPHERE BY USE OF SOLAR OCCULTATION AS SEEN FROM AN ARTIFICIAL SATELLITE

By H. Andrew Wallio and James R. Williams
Langley Research Center

SUMMARY

A feasibility study to determine the physical properties of the Martian atmosphere by the occultation of sunlight as seen by an artifical satellite has been conducted. Five model atmospheres have been used in this study. The effects of refraction, Rayleigh scattering, and limb darkening and finite sun size have been included in the mathematical model for visible light passing through the atmosphere. The study has shown that the technique of using the occultation of the sun as seen by an artificial satellite does provide a means of determining the physical properties of the Martian atmosphere provided that a differential correction technique to match observational data with theoretical data is developed. This report also shows the importance of using the shorter wavelengths of visible light since the observed effects are most pronounced in this region of the spectrum.

INTRODUCTION

Currently, there are several unmanned vehicles planned for the exploration of the planet Mars. These vehicles will be used to gather data concerning the physical properties of the planet. One of the primary areas of research will be the determination of the constituents of the Martian atmosphere and their distribution. This report presents a relatively simple technique which should be considered as a means of determining such atmospheric properties as surface pressure and scale height. The technique employed utilizes the observed light-intensity variation from the sun as the light passes at grazing incidence through the planetary atmosphere.

The theory describing the observed optical effects that occur during an eclipse of a satellite by a planet with an atmosphere is given by Link. (See ref. 1.) The application of occultation to the observed light intensity of the moon of a planet is discussed by Rakos (ref. 2) and Weisberg (ref. 3). The effects of scattering (refs. 4 and 5), absorption (ref. 6), and the finite size of the sun (refs. 1 and 3) must also be taken into account when the lower regions of the atmosphere are viewed.

Since this paper is primarily a feasibility study, only the primary factors determining the variation of light intensity have been included. These factors are refraction through the atmosphere, limb darkening, finite sun size, and Rayleigh scattering. Light-intensity-variation curves are presented for each of these effects considered both singly and collectively. The curves presented are for five model atmospheres and for a range of four wavelengths of visible light. Also a short discussion of the effect of the distance of the satellite from the planet is included.

This technique utilizing the occultation of sunlight as seen by an artificial satellite can be used as an independent data type to determine scale height and surface pressure or to provide a check on any other independent data source. The advantage of occultation data is that by assuming an attitude control system and cruise orientation similar to that used on the lunar orbiter and Mariner spacecraft, one spacecraft axis would nominally be pointing toward the sun, and sensors properly mounted would require no additional attitude control. Also the use of an orbiter results in a number of observations and would allow a study of the effects due to clouds or dust since there should be a large number of observations that would be essentially cloud and dust free.

SYMBOLS

B	normalized coefficient in limb darkening
D	distance from trajectory to planet (see fig. 2)
ds, ds'	differential spacing of adjacent light rays (see fig. 3)
F(D,x)	integrated intensity due to finite size of sun
f(D,x)	intensity of light at point x a distance D from planet due to a point source at center of sun
f_j	coefficient of depolarization of jth gas
g	acceleration due to gravity, 3.7 m/sec^2
h	pressure scale height, $\frac{R_o T_o}{mg}$, km
I	intensity of light
L(y)	limb darkening of sun

l	path length, km
$l(y)$	factor determining solar shape and limb darkening
m	average mass of gas, kg/mole
n	index of refraction
p	atmospheric pressure, bars $\left(1 \text{ bar} = 10^5 \text{ N/m}^2\right)$
R	gas constant per unit mass
R_o	universal gas constant
r	radius of planet, km
T	temperature, ^oK
V	variable limit of integration
x	coordinate of satellite trajectory, km
y	integration variable over solar disk
Z	altitude above surface of planet, km
α	half-angle subtended by sun as seen from satellite, radians
β	Rayleigh scattering coefficient, km^{-1}
Γ	temperature gradient, km^{-1}
γ	angle between line of sight to sun and sun planet line, radians
δ	first variation
ϵ	refractivity
η_o	Loschmidt's number
θ	angle between minimum altitude and radius to satellite, radians

λ wavelength of light, km

μ constant of integration

ν fraction by volume of ith gas

ρ atmospheric density, kg/km^3

τ optical depth

ω deviation of light ray from straight line, radians

Subscripts:

e earth surface conditions

i incident or initial conditions

j summation index over number of gas constituents

o Martian surface conditions

1 values at minimum altitude

ASSUMPTIONS AND ANALYSIS

The construction of a mathematical model in order to perform a feasibility study for the use of solar occultation data as a method of determining the physical properties of the Martian atmosphere has required certain assumptions which are outlined as follows:

(1) The sun, planet, and satellite are all coplanar (fig. 1)

(2) The planet is a sphere of radius r

(3) The distance into the geometric shadow x is small compared with the distance from the observer to the center of the planet (See fig. 2.)

(4) The radius of the planet is much greater than any characteristic height in the atmosphere

(5) The atmosphere is a perfect gas of uniform chemical composition in hydrostatic equilibrium

(6) The refractivity is small compared with unity

(7) The change in temperature is small over an altitude distance of one scale height

The temperature profiles assumed are a least-squares linear fit, between 0 and 100 km above the Martian surface, to the temperature curves of the Martian atmosphere engineering models used by the Viking Project. The basic properties of the atmosphere are given in table I. These models as presented in table I provide the basis for this feasibility study and are the only models discussed herein. It is further assumed that the source is a finite disk and sufficiently far from the planet so that the incident light may be considered to be plane waves. The final assumption is that multiple scattering and Mie scattering are negligible. The possible importance of Mie scattering is discussed in reference 7.

In this paper the three major effects upon the variation of light intensity are refraction through the Martian atmosphere, limb darkening of the sun, and Rayleigh scattering due to the gas molecules in the atmosphere.

The first effect under consideration is that of differential refraction which causes the divergence of two infinitesimally separated parallel rays as they traverse an atmosphere whose index of refraction is a function of the altitude. Figure 3 shows two incident parallel rays of separation ds which traverse the atmosphere and emerge with a separation ds' which is greater than ds. Thus an incident beam with an intensity I_i and an infinitesimal separation ds has a flux proportional to $I_i\, ds$. Since the flux entering the tube shown in figure 3 must be equal to the flux emerging at the observation point, it follows that

$$I = I_i \frac{ds}{ds'} \tag{1}$$

Therefore the intensity at the point of observation will necessarily be less than the incident intensity. The spreading of the beam and the derivation showing the dependence of the spreading on the constituents and physical properties of the atmosphere are given in appendix A.

Another effect which causes a diminution in the observed light intensity is due to the limb darkening of the sun. The light which reaches the satellite is a sum of contributions from the various parts of the disk of the sun, each passing through a different layer of the Martian atmosphere. The effect is a spreading of the light curve and a smoothing of the discontinuities due to the fine structure of the atmosphere. Implicit in limb-darkening effects is the consideration of the fact that the sun has a finite size. These two effects are included in this occultation analysis, and their derivations are included in appendix B.

The third major effect taken into account is that of Rayleigh scattering which is the scattering of light from the gas molecules in the atmosphere. Rayleigh discovered that for scattering in which the wavelength of the incident electromagnetic radiation is long in comparison with the dimensions of the scatterer, the scattering is dependent upon the fourth power of the wavelength. Radiation traversing the atmosphere suffers loss due to absorption and scattering. For this paper the effects of absorption were considered to be negligible in comparison with Rayleigh scattering. The intensity of a parallel beam of light decreases, because of the extinction process, by a factor of

$$I = I_i e^{-\beta l} \tag{2}$$

where β is a local extinction coefficient derived by Rayleigh and l is the path length. The complete derivation of the dependencies of the physical properties of the atmosphere on β and l is given in appendix C.

RESULTS AND DISCUSSION

In order to facilitate the discussion, it is convenient to classify the various model atmospheres under study. Table I presents a list of the five models, used in this feasibility study, along with their constant physical properties. Throughout the remainder of this text, these models are referred to according to the numbers given in table I.

Since this study is a feasibility study, a circular orbit of 8700 km was chosen arbitrarily for the radius of the satellite orbit. For the effects which are dependent upon the distance from the planet, a separate discussion is included but, in general, the 8700-km circular orbit is of primary importance.

In order to present a deeper insight into the effect of refraction, Rayleigh scattering, and limb darkening, each of these effects has been studied independently and in combinations with each other.

The effect of refraction only is the first of these areas to be studied. Since for a low-density gas, the refraction is essentially independent of wavelength, wavelength is not included in figure 4. Figure 4 is a plot of the ratio of light-intensity variation as a function of the distance into the geometrical shadow of the planet (see fig. 2) for the effect of refraction only. These curves are for a satellite in an 8700-km circular orbit. The significance of scale height and, in this case, surface temperature is illustrated in the difference in light-intensity variation in figures 4(a) and 4(b) and in the difference in light-intensity variation in figures 4(d) and 4(e). The only differences in physical properties of figures 4(a) and 4(b) are surface-temperature conditions in which there is a 100° K difference and a small difference in the slope of the temperature profiles, likewise for

figures 4(d) and 4(e). Figure 4(c) represents the light-intensity variation for the so-called "most probable model." Note that in figure 4 all the light-intensity curves are terminated at approximately the same point. From equation (A29), it can be shown that for D = 8700 km, the point at which the light intensity drops to zero is approximately 26.6 km. As would be expected, model IV gives the greatest variation in light-intensity distribution since it has the lowest surface temperature and the highest surface pressure of any of the models. Note in connection with figure 4 that the light intensity drops very slowly until it reaches a point at which it disappears completely. This effect is precisely the expected effect from considerations of refraction only from a finite source.

The effect of limb darkening and finite size of the sun as discussed in appendix B is independent of wavelength. In order to best illustrate the effect of limb darkening and finite sun size on the light intensity, a computation was made for a planet with no atmosphere. Figure 5 illustrates this effect for a satellite in a 8700-km circular orbit. As can be seen from figure 5, the light-intensity ratio drops from 1.0 to zero gradually over a distance of approximately 56 km. Since the effects of considering the finite size and the limb darkening of the sun are dependent upon the angle which the sun subtends as seen from the satellite, figure 6 illustrates this distance-dependent effect. As can be seen from figure 6, the greater the satellite orbital radius, the slower the light-intensity-ratio curves drop to zero.

The next area of interest in this study is the effect of Rayleigh scattering. Figure 7 illustrates the effect of Rayleigh scattering which is proportional to the inverse fourth power of wavelength. In order to illustrate the effect of Rayleigh scattering better, figure 7 includes only Rayleigh scattering effects. In figure 7 it can be seen that the shorter wavelengths for a given model tend to suffer the greatest reduction in intensity. A note concerning figure 7 is that at approximately 26.6 km, the light is physically blocked from the satellite by the planet. Therefore, at this point the ratio of light intensity drops to zero. The effect of scale height can readily be seen in the difference between the curves in figures 7(a) and 7(b) where the major difference in models is the 100° K difference in surface temperature, and the small difference in the slope of the temperature profiles, likewise for figures 7(d) and 7(e). Figure 7(c) again presents the Rayleigh scattering effect for the most probable model. The effect of surface pressure as well as scale height is apparent in the difference between figures 7(a) and 7(e), and in the difference between figures 7(b) and 7(d). Note in comparing these figures that the vertical scale is not the same for all models. The effects shown in figures 7(a) and 7(e) and in figures 7(b) and 7(d) reflect the dependence of the Rayleigh scattering coefficient on density as can also be seen in the derivation in appendix C.

Now that the magnitude and the importance of the single effects considered in this report have been discussed, it is necessary to combine the effects in order to obtain the

results of this study. For the sake of brevity, the summation of the effect of refraction, Rayleigh scattering, and limb darkening and finite sun size is hereafter referred to as the combined effects. In order to obtain the combined effects at any given point x, one simply takes the value of the light-intensity ratio at that point from each of the curves illustrating the single effect (figs. 4, 5, and 7) and forms their product. This product produces the resultant light-intensity variation for figures 8 to 11.

Figure 8 is a plot of the variation of the light-intensity ratio with the distance of the satellite into the geometric shadow for a received light intensity of 6500 angstroms with the combined effects. In order to facilitate the discussion, it is convenient at this point to use the scale height h which is a surface-pressure scale height, as a factor for discussing each of the models. The scale height associated with each of the models is presented in table I. Figures 8(a) and 8(b) are models which have the same physical properties except for a difference of 100° K in surface temperature and a difference in the slope of the temperature profile. This difference is reflected in a scale-height difference of approximately 5 km. For figures 8(a) and 8(b), the surface pressure of which is low (4 mb), the effect of a scale-height difference is small and only visually detectable in the region between -40 and -20 km into the shadow. Basically, the same observation may be made for figures 8(d) and 8(e); the only difference is a scale-height difference of approximately 6.8 km. However, for figures 8(d) and 8(e), the surface pressure is 20 mb, and the difference in the light-intensity variation in the -40 to -20 km region of the shadow is more perceptible. Figure 8(c) is the light-intensity variation for the atmospheric model which reference 1 calls the most probable model. The differences among figures 8(a), 8(c), and 8(d) are easily perceptible even though their scale heights are within 2.6 km of each other. This difference is attributed chiefly to their surface-pressure differential.

Figures 9 and 10 present the same combined effects as were presented in figure 8 except that figure 9 is for wavelengths of 5500 angstroms and figure 10 is for a wavelength of 4700 angstroms. One of the basic reasons for including figures 9 and 10 is for a reference in case a cross plot involving wavelength is desired by the reader.

Figure 11 is a plot of the variation of light-intensity ratio with the depth into the geometrical shadow for a wavelength of 3500 angstroms. Figures 11(a) and 11(b) as were figures 8(a) and 8(b), 9(a) and 9(b), and 10(a) and 10(b) are presented for models the only difference of which is in scale height. However, it should be noted that in figures 11(a) and 11(b), the difference between these two figures in the -40 to -20 km range is more perceptible. This effect is very obvious for figures 11(d) and 11(e). Again the scale height differs by 6.8 km; however, the difference in light curves is much more predominant at the shorter wavelengths. This condition is a result of the Rayleigh scattering being inversely proportional to the fourth power of wavelength.

The results of this study can best be discussed with the aid of figures which contain the superposition of some previously presented curves. These curves illustrate the difference in the light-intensity variation for the extremes in visible light and illustrate the ease with which model atmospheres can be distinguished when the lower wavelengths of visible light are used.

Figure 12(a) is a superposition of figures 8(a), 8(c), and 8(d) which are for a wavelength of 6500 angstroms and a surface pressure of 4 mb, 9 mb, and 20 mb, respectively. The scale-height differential between models I and III is 1.2 km with a surface-pressure differential of 5 mb. From figure 12(a), it can be seen that this value produces approximately a 2-percent maximum difference in light curves. On the other hand, the scale-height difference between models III and IV is 1.4 km with a pressure differential of 11 mb. This value produces a maximum variation in the light-intensity curve of approximately 6 percent. Thus, if the scale height were known, the light sensor would require 0.5-percent accuracy to determine surface pressures within 2 to 3 mb at 6500 angstroms.

Figure 12(b) is a superposition of figures 8(d) and 8(e) showing that at 6500 angstroms, a scale-height differential of 6.8 km results in a 3-percent maximum difference in light-intensity variation at a constant surface pressure of 20 mb.

Figure 13(a) is a superposition of figures 11(a), 11(c), and 11(d) for a wavelength of 3500 angstroms and a surface pressure of 4 mb, 9 mb, and 20 mb, respectively. With a surface-pressure differential of 5 mb and a scale-height differential of 1.2 km between models I and III, it can be seen from figure 13(a) that the light-intensity variation differs by a maximum of 11 percent. For a scale-height difference of 1.4 km and a surface-pressure differential of 11 mb for models III and IV, figure 13(a) shows a 33-percent maximum difference in light-intensity variation. Furthermore, there is a maximum difference of 44 percent in the light-intensity variation for models I and IV as shown in figure 13(a) for which the scale-height differential is 2.6 km and the surface-pressure differential is 16 mb.

Figure 13(b) is a plot of figures 11(d) and 11(e) for the wavelength of 3500 angstroms and a surface pressure of 20 mb. The difference in scale height is 6.8 km which leads to a 11-percent difference in light-intensity curves. Thus, the advantage of performing this experiment with the shorter (3500 angstroms) wavelengths is adequately illustrated in figures 12 and 13.

There are some general observations that can be made concerning figures 8 to 13. It appears that the surface pressure can be approximated by following the slope of the curves in the -60 to -20 km range, the higher rate of change of the slope in the region of the knee of the curve denoting the lower pressures. For curves with the same surface pressure and with the same wavelength of received light but different scale heights, the

curve with the lower scale height intersects the curve with higher scale height from above as shown in figure 13(b). These facts are mentioned because they would provide a basis for the formulation of a differential correction method to determine scale height and surface pressure from observational data. On the other hand, if one is provided with scale height by some external measurement, this technique will provide a method of determining surface pressure.

CONCLUDING REMARKS

This study has included the effects of refraction, limb darkening, finite sun size, and Rayleigh scattering. These effects have been considered singly and collectively. Singly, both refraction and Rayleigh scattering show effects of scale-height differences; however, limb darkening and finite sun sizes are the dominant effects in the light-intensity variation, and the predominance of scattering over refraction effects on the light curves has been shown. In using the occultation of the sun as seen by an artificial satellite as means of determining the physical properties of the Martian atmosphere, it has been shown that the most predominant effect, a 44-percent variation in light intensity, is observed when visible light of short wavelengths (3500 angstroms) is used.

This technique of occultation can provide the means of determining the physical properties, scale height, and surface pressure. However, the technique would depend upon the development of a differential correction technique to match the observed curves with the theoretical curves. However, this study has shown that the technique is a feasible one for determining the physical properties of the Martian atmosphere and warrants further study and consideration.

Langley Research Center,
National Aeronautics and Space Administration,
Langley Station, Hampton, Va., June 17, 1969.

APPENDIX A

ATMOSPHERIC REFRACTION OF LIGHT

The vertical distribution of pressure in a fluid can be expressed in terms of the hydrostatic equation

$$dp = -g\rho\, dZ \tag{A1}$$

Since an atmosphere consists of a compressible gas, its density is a function of altitude

$$\rho = \rho(Z) \tag{A2}$$

Gravity too is a function of altitude above the planet's surface; however, for this paper it was assumed to be a constant.

In order to establish the variation of density with altitude, it is assumed that the atmosphere obeys the ideal gas law:

$$p = \rho RT \tag{A3}$$

where

$$R = \frac{R_o}{m} \tag{A4}$$

Temperature is assumed to vary linearly with altitude over the pertinent range

$$T = T_o(1 + \Gamma Z) \tag{A5}$$

where T_o is the surface temperature and $T_o\Gamma$ is the slope. Substituting equation (A5) into equation (A3) yields

$$\rho = \frac{p}{RT} = \frac{p}{RT_o(1 + \Gamma Z)} \tag{A6}$$

Substituting equation (A6) into equation (A1) yields

$$\int_{p_o}^{p} \frac{dp}{p} = -\int_0^Z g \frac{dZ}{RT_o(1 + \Gamma Z)} \tag{A7}$$

APPENDIX A

The integral in equation (A7) gives

$$p = p_o \exp\left[-\frac{g}{RT_o}\left(Z - \frac{\Gamma}{2}Z^2\right)\right]$$

where

$$\frac{1}{1 + \Gamma Z} \approx 1 - \Gamma Z \tag{A8}$$

has been used.

The index of refraction for a rare gas may be written as

$$n(Z) = 1 + \epsilon(Z) \tag{A9}$$

where $\epsilon(Z)$ is the refractivity as given by the Lorenz-Lorentz formula which states that the refractivity is proportional to the density of the gas. Therefore,

$$\epsilon(Z) = \frac{\epsilon_o}{\rho_o}\rho(Z) \tag{A10}$$

Substituting equation (A6) into equation (A10) yields

$$\epsilon(Z) = \epsilon_o(1 - \Gamma Z)\exp\left[-\frac{g}{RT_o}\left(Z - \frac{\Gamma}{2}Z^2\right)\right] \tag{A11}$$

where ϵ_o may be evaluated from standard temperature and pressure conditions at the earth's surface by using the relation

$$\epsilon_o = \epsilon_e \frac{p_o T_e}{T_o p_e} \tag{A12}$$

The path of a ray of light passing through a planetary atmosphere can be found from Fermat's principle

$$\delta \int n(Z)\, ds = 0 \tag{A13}$$

where

$$ds^2 = dZ^2 + (r + Z)^2\, d\theta^2$$

The Euler-Lagrange equation which yields the minimum for equation (A13) is

APPENDIX A

$$\frac{n(Z)(r + Z)^2 \frac{d\theta}{dZ}}{\left[1 + (r + Z)^2\left(\frac{d\theta}{dZ}\right)^2\right]^{1/2}} = \text{Constant} = \mu \tag{A14}$$

At the point of closest approach, Z_1, $\frac{dZ}{d\theta} = 0$, therefore

$$\mu = (1 + \epsilon_1)(r + Z_1) \tag{A15}$$

Substituting equation (A15) into equation (A14) and integrating yields

$$\theta(Z) = \int_{Z_1}^{Z} \frac{(1 + \epsilon_1)(r + Z_1)\, dZ}{(r + Z)\left[(1 + \epsilon)^2(r + Z)^2 - (1 + \epsilon_1)^2(r + Z_1)^2\right]^{1/2}} \tag{A16}$$

From figure 14, it can be seen from the geometry that

$$\frac{\omega}{2} + \frac{\pi}{2} = \theta(\infty) \tag{A17}$$

and

$$\frac{\pi}{2} \equiv \int_{Z_1}^{\infty} \frac{(r + Z_1)\, dZ}{(r + Z)\left[(r + Z)^2 - (r + Z_1)^2\right]^{1/2}} \tag{A18}$$

Then it follows that

$$\omega(Z_1) = 2 \int_{Z_1}^{\infty} \frac{r + Z_1}{r + Z} \left\{ \frac{\left(2rZ - 2rZ_1 + Z^2 - Z_1^2\right)^{1/2}}{\left[\left(\frac{1 + \epsilon}{1 + \epsilon_1}\right)^2 (r + Z)^2 - (r + Z_1)^2\right]^{1/2}} - 1 \right\} \Big/ \left(2rZ - 2rZ_1 + Z^2 - Z_1^2\right)^{1/2} dZ \tag{A19}$$

If it is assumed that when the integrand is large,

(a) $\epsilon_1 \ll 1$

(b) $r \gg |Z - Z_1|$

(c) $r \gg Z$

(d) $r\left|\frac{\epsilon - \epsilon_1}{Z - Z_1}\right| \ll 1$

then,

$$\omega(Z_1) = \sqrt{\frac{2}{r}} \int_{Z_1}^{\infty} \frac{1}{(Z - Z_1)^{1/2}} \left[\left(1 + \frac{\epsilon - \epsilon_1}{Z - Z_1} r \right)^{-1/2} - 1 \right] dZ \tag{A20}$$

By using approximation (d), equation (A20) becomes

$$\omega(Z_1) \approx \sqrt{\frac{r}{2}} \int_{Z_1}^{\infty} \frac{\epsilon_1 - \epsilon}{(Z - Z_1)^{3/2}} \left(1 + \frac{3}{4} \frac{\epsilon_1 - \epsilon}{Z - Z_1} r + \ldots \right) dZ \tag{A21}$$

By using equation (A11) in equation (A21),

$$\omega(Z_1) \approx \epsilon_1 \sqrt{\frac{r}{2}} \int_{Z_1}^{\infty} \left(\frac{1 - \exp\left(\frac{Z - Z_1}{h_1} \right)}{(Z - Z_1)^{3/2}} + \Gamma \frac{\exp\left(- \frac{Z - Z_1}{h_1} \right)}{(Z - Z_1)^{1/2}} + \frac{3}{4} \epsilon_1 r \frac{\left\{ 1 - \exp\left[- \left(\frac{Z - Z_1}{h_1} \right) \right] \right\}^2}{(Z - Z_1)^{5/2}} \right) \tag{A22}$$

where

$$h_1 = \frac{RT_1}{g}$$

Integrating equation (A22) yields

$$\omega(Z_1) = \epsilon_1 \sqrt{\frac{2\pi r}{h_1}} \left[1 + \frac{\Gamma h_1}{2} + \left(\sqrt{2} - 1 \right) \frac{\epsilon_1 r}{h_1} \right] \tag{A23}$$

Generalizing equation (A23) for any altitude allows the subscript 1 to be dropped.

$$\omega(Z) = \epsilon \sqrt{\frac{2\pi r}{h}} \left[1 + \frac{\Gamma h}{2} + \left(\sqrt{2} - 1 \right) \frac{\epsilon r}{h} \right] \tag{A24}$$

The ratio of incident to received intensity is equal to the ratio of ds' to ds or

$$\frac{I}{I_i} = \frac{ds}{ds'} \tag{A25}$$

From figure 15, it can be seen that approximately

$$\frac{I}{I_i} = \frac{ds}{ds + D\, d\omega} \tag{A26}$$

or

$$\frac{I}{I_i} = \frac{ds}{ds + D\left|\frac{d\omega(Z_1)}{dZ}\right| ds} = \left(1 + D\left|\frac{d\omega}{dZ_1}\right|\right)^{-1} \tag{A27}$$

Combining equations (A11) and (A24) gives

$$\omega(Z) = \omega_1\left(1 - \frac{3}{2}\Gamma Z\right)\exp\left[-\frac{1}{h_1}\left(Z - \frac{\Gamma}{2}Z^2\right)\right] \tag{A28}$$

Thus

$$\frac{I}{I_i} = \left\{1 + \frac{\omega_1 D}{h_1}\left(1 + \frac{3}{2}\Gamma h_1 - \frac{5}{2}\Gamma Z\right)\exp\left[\frac{-\left(Z - \frac{\Gamma}{2}Z^2\right)}{h_1}\right]\right\}^{-1} \tag{A29}$$

which is the result used in equation (1) of the text. For further discussion see references 3 and 4. An alternate approach to the same form is given in reference 8.

APPENDIX B

LIMB DARKENING AND THE FINITE SIZE OF THE SUN

The light from the sun which reaches a satellite is the sum of contributions from various parts of the sun, each ray passing through a different layer of the atmosphere. This condition results in a spreading of the light curve and a smoothing of the discontinuities due to the fine structure in the atmosphere.

To account for this effect, assume that the distance D in figure 16 is a constant and the distance x is a variable function of the direction of the light ray emanating from the sun.

If $f(D,x)$ is the intensity at point x for a point source located at the center of the sun, the integrated intensity due to the finite size of the sun is of the form

$$F(D,x) = \int_{-1}^{1} f(D, x+\alpha Dy)l(y)\, dy \tag{B1}$$

which is given in reference 2. The half-angle α subtended by the sun as seen from x and $l(y)$ is a function which takes into account both the circular shape and the limb darkening of the sun.

By assuming that the brightness of a segment of the sun is given by the product $l(y)\, dy$ where dy is the segment width, the total light intensity of the sun is

$$\int_{-1}^{1} l(y)\, dy = 1 \tag{B2}$$

Let $L(\cos \gamma)$ denote the factor giving the intensity of solar limb darkening where γ is the angle between the line of sight to the sun at x and the normal to the sun; then in terms of x and y

$$\cos \gamma = \left[1 - \left(x^2 + y^2\right)\right]^{1/2} \tag{B3}$$

where x and y as they appear here are normalized to the radius of the sun. The function $l(y)$ can be expressed as the fraction of the light intensity received at dx due to the solar element dy. This condition results in

$$l(y) = \frac{\int_{-\sqrt{1-y^2}}^{\sqrt{1-y^2}} L\left(\sqrt{1 - x^2 - y^2}\right) dx}{\int_{-1}^{1} \int_{-\sqrt{1-y^2}}^{\sqrt{1-y^2}} L\left(\sqrt{1 - x^2 - y^2}\right) dx\, dy} \tag{B4}$$

where the term in the denominator is a normalization factor as given in reference 2. By following reference 3 and assuming that $L(\cos \gamma)$ is of the form

$$L(\cos \gamma) = B + (1 - B) \cos \gamma \tag{B5}$$

equation (B4) becomes

$$\mathcal{l}(y) = \frac{3}{\pi(B + 2)}\left[2B\sqrt{1 - y^2} + \frac{\pi}{2}(1 - B)\left(1 - y^2\right)\right] \tag{B6}$$

This expression is substituted into the final form for the light intensity in appendix C.

APPENDIX C

RAYLEIGH SCATTERING

Radiation transversing a planetary atmosphere suffers losses in intensity due to absorption and to scattering in other directions. This effect is called extinction. Since the Martian atmosphere is rare, absorption has been neglected in this report.

Atmospheric scattering will reduce the intensity of the incident light as given by

$$I = I_i e^{-\tau} \tag{C1}$$

where τ is the optical thickness of the atmosphere and is given by

$$\tau = \int_0^l \beta \, dl \tag{C2}$$

β is the Rayleigh scattering coefficient, and dl is the differential path length. From reference 5 β is given by

$$\beta = \frac{32\pi^3}{3\lambda^4 \eta_o} \sum_j \nu_j \left[n_j(Z) - 1\right]^2 f_j \tag{C3}$$

But

$$\left[n_j(Z) - 1\right]^2 = \left[\epsilon_j(Z)\right]^2 \tag{C4}$$

$$\left[n_j(Z) - 1\right]^2 = \left\{\epsilon_{oj}(1 - \Gamma Z) \exp\left[-\frac{1}{h_o}\left(Z - \frac{\Gamma}{2} Z^2\right)\right]\right\}^2 \tag{C5}$$

$$\left[n_j(Z) - 1\right]^2 \approx \left(\epsilon_{oj}\right)^2 e^{\frac{-2Z}{h_o}} \tag{C6}$$

From the geometry (fig. 14)

$$l^2 \approx (r + Z)^2 - \left(r + Z_1\right)$$

and in the region where $\int \beta \, dl$ is large, $r >> Z + Z_1$ so that $l^2 \approx 2r\left(Z - Z_1\right)$ and

APPENDIX C

$$\exp\left(-\frac{2Z}{h_o}\right) = \exp\left[-\frac{2}{h_o}(Z - Z_1) - \frac{2Z_o}{h_o}\right] \approx \exp\left(-\frac{2}{h_o}\frac{\ell^2}{2r_o} - \frac{2Z_1}{h_o}\right) \tag{C7}$$

Since, the number density η_o approaches $\eta_o \exp\left(-\frac{\ell^2}{2rh_o} - \frac{Z_1}{h_o}\right)$ the optical depth becomes

$$\tau \approx 2\int_0^\infty \frac{32\pi^3}{3n_o\lambda^4} e^{\frac{-Z_1}{h_o}} \sum_j \nu_i f_j(\epsilon_{oj})^2 e^{\frac{-\ell^2}{2h_o r}}\, d\ell \tag{C8}$$

Collecting constant terms yields

$$\tau = 2\frac{32\pi^3}{3n_o\lambda^4}\exp\left(-\frac{Z_1}{h_o}\right)\sum_j \nu_j f_j(\epsilon_{oj})^2 \int_0^\infty \exp\left(-\frac{\ell^2}{2h_o r}\right) d\ell \tag{C9}$$

$$\tau = \frac{32\pi^3}{3n_o\lambda^4}\exp\left(-\frac{Z_1}{h_o}\right)\sum_j \nu_j f_j(\epsilon_{oj})^2 \sqrt{2\pi r h_o} \tag{C10}$$

The constant terms correspond to the scattering coefficient at the surface, therefore, the optical depth reduces to

$$\tau = \beta_o\sqrt{2\pi r h_o}\exp\left(-\frac{Z_1}{h_o}\right) \tag{C11}$$

where $\beta_o = \frac{32\pi^3}{3n_o\lambda^4}\sum_j \nu_j f_j(\epsilon_{oj})^2$.

The primary effect of Rayleigh scattering is to vary the initial slope of the intensity curve as a function of the wavelength. Thus there should be a distinct intensity curve for each wavelength measured from the satellite. By combining the equations for refraction, Rayleigh scattering, and finite solar size, the final form for the equation of the light intensity as a function of x is

$$\frac{I(x)}{I_i} = \begin{cases} \dfrac{\exp\left\{-\beta_o\sqrt{2\pi r h_o}\left[\exp\left(-\frac{Z}{h_o}\right)\right]\right\}}{1 + \frac{\omega_o D}{h_o}\left(1 + \frac{3}{2}\Gamma h_o - \frac{5}{2}\Gamma Z\right)\exp\left(-\frac{Z}{h_o}\right)} \int_{-1}^{V} \ell(y)\, dy & \left(0 < Z < Z_{max}\right) \\ 0 & (Z \leq 0) \end{cases} \tag{C12}$$

where

$$x + \alpha Dy = -Z + \omega_o D\left(1 + \frac{3}{2}\Gamma h_o - \frac{5}{2}\Gamma Z\right)e^{\frac{-Z}{h_o}} \tag{C13}$$

and

$$V = \begin{cases} 1 & \left(1 \leqq \frac{1}{\alpha D}\left[\omega_o D\left(1 + \frac{3}{2}\Gamma h_o\right) - x\right]\right) \\ \frac{1}{\alpha D}\left[\omega_o D\left(1 + \frac{3}{2}\Gamma h_o\right) - x\right] & \left(-1 \leqq \frac{1}{\alpha D}\left[\omega_o D\left(1 + \frac{3}{2}\Gamma h_o\right) - x\right] \leqq 1\right) \\ -1 & \left(-1 \geqq \frac{1}{\alpha D}\left[\omega_o D\left(1 + \frac{3}{2}\Gamma h_o\right) - x\right]\right) \end{cases}$$

REFERENCES

1. Link, F.: Eclipse Phenomena. Advances in Astronomy and Astrophysics, Vol. 2, Zdeněk Kopal, ed., Academic Press Inc., c.1963, pp. 87-198.

2. Rakos, Karl D.: The Atmospheric Pressure at the Surface of Mars. Lowell Observatory Bull., No. 131, vol. VI, no. 12, 1968, pp. 221-231.

3. Weisberg, H. L.: The Study of Planetary Atmospheres by Stellar Occultation. RM-3279-JPL (Contract N-33561 (NAS 7-100)), Rand Corp., Oct. 1962.

4. Menzel, Donald H.: Optical Refraction in a Planetary Atmosphere With Application to the Apparent Diameter of a Planet and to Occultation. GCA Tech. Rep. 61-33-A (Contract AF 33(616)-7413), Geophysics Corp. America, July 1961.

5. Kuiper, Gerard P. (editor): The Atmospheres of the Earth and Planets. Univ. Chicago Press, c.1952.

6. Chandrasekhar, C.: Radiative Transfer. Dover Pub., Inc., c.1960.

7. Rakos, Karl D.: The Atmospheric Pressure at the Surface of Mars. Moon and Planets, A. Dollfus, ed., North-Holland Pub. Co., 1967, pp. 256-261.

8. De Vaucouleurs, Gérard: Planetary Astronomy From Satellite-Substitute Vehicles-II, A Survey of Physical Problems of the Nearer Planets and a Review of Observational Techniques Applicable to Balloon-Borne Telescope Systems. AFMDC-TN-59-37, U.S. Air Force, Dec. 1959. (Available from DDC as AD 233561.)

TABLE I.- SUMMARY OF CONDITIONS AT MEAN SURFACE FOR FIVE MODEL ATMOSPHERES

Atmosphere	Atmospheric conditions										Pressure scale height, km
	Surface pressure, mb	Surface temperature, ^{o}K	Composition by mass, percent			Composition by volume, percent			Molecular mass, kg/kg-mole	Γ, km^{-1}	
			CO_2	N_2	Ar	CO_2	N_2	Ar			
Model I	4	262	100	0	0	100	0	0	44	-6.42×10^{-3}	13.38
Model II	4	160	100	0	0	100	0	0	44	-4.59×10^{-3}	8.11
Model III	9	219	74.4	12.8	12.8	68.5	18.5	13.0	40.5	-3.99×10^{-3}	12.17
Model IV	20	160	25	50	25	19	60	21	33.6	-3.08×10^{-3}	10.77
Model V	20	262	25	50	25	19	60	21	33.6	-5.23×10^{-3}	17.56

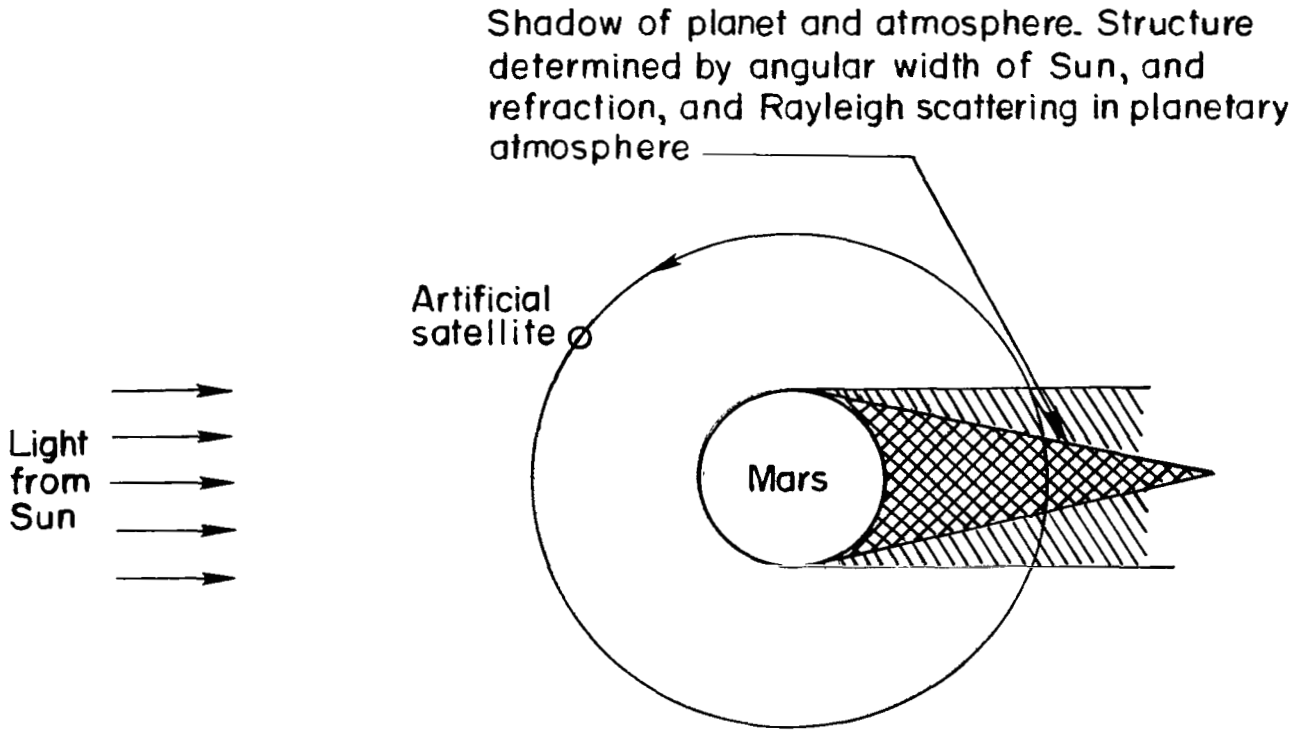

Figure 1.- Configuration for occultation.

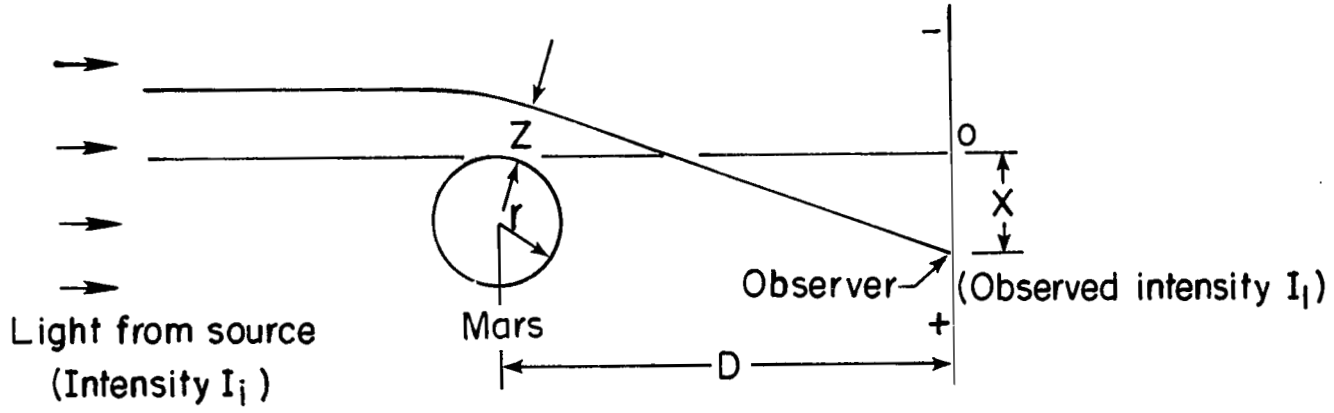

Figure 2.- Configuration of source, planet, and observer.

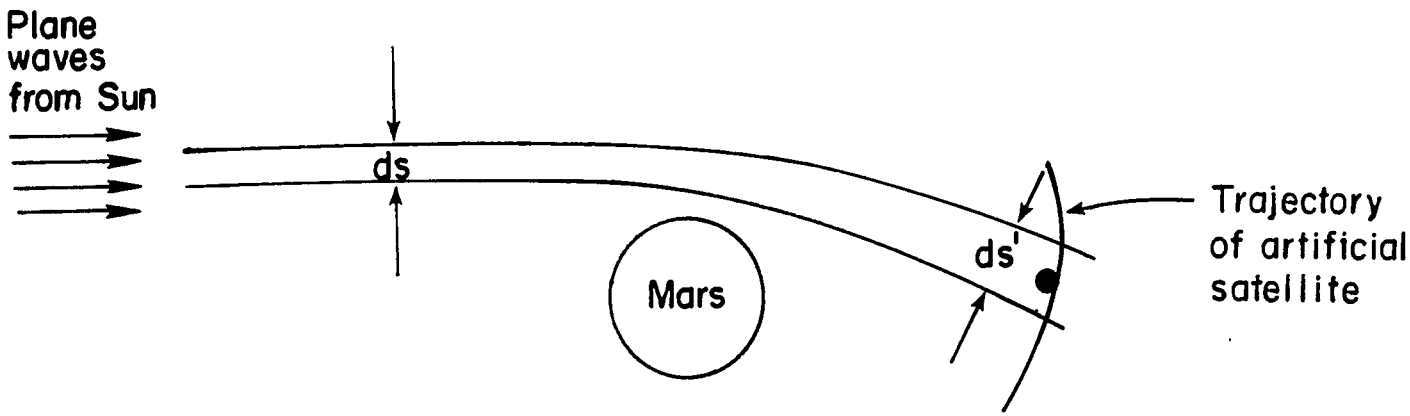

Figure 3.- Differential refraction configuration.

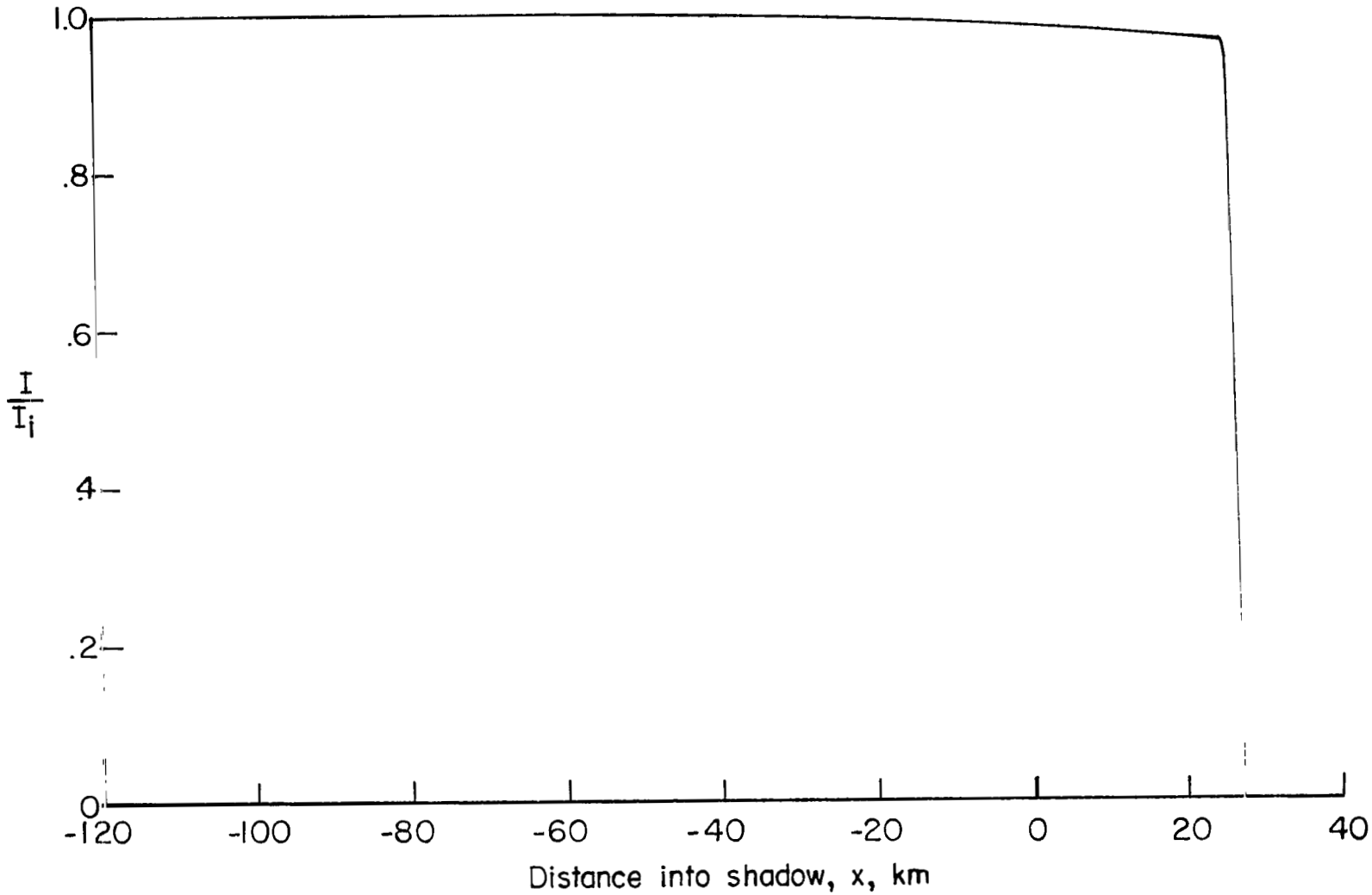

(a) Model I; D = 8700 km.

Figure 4.- Light intensity variation due to refraction only.

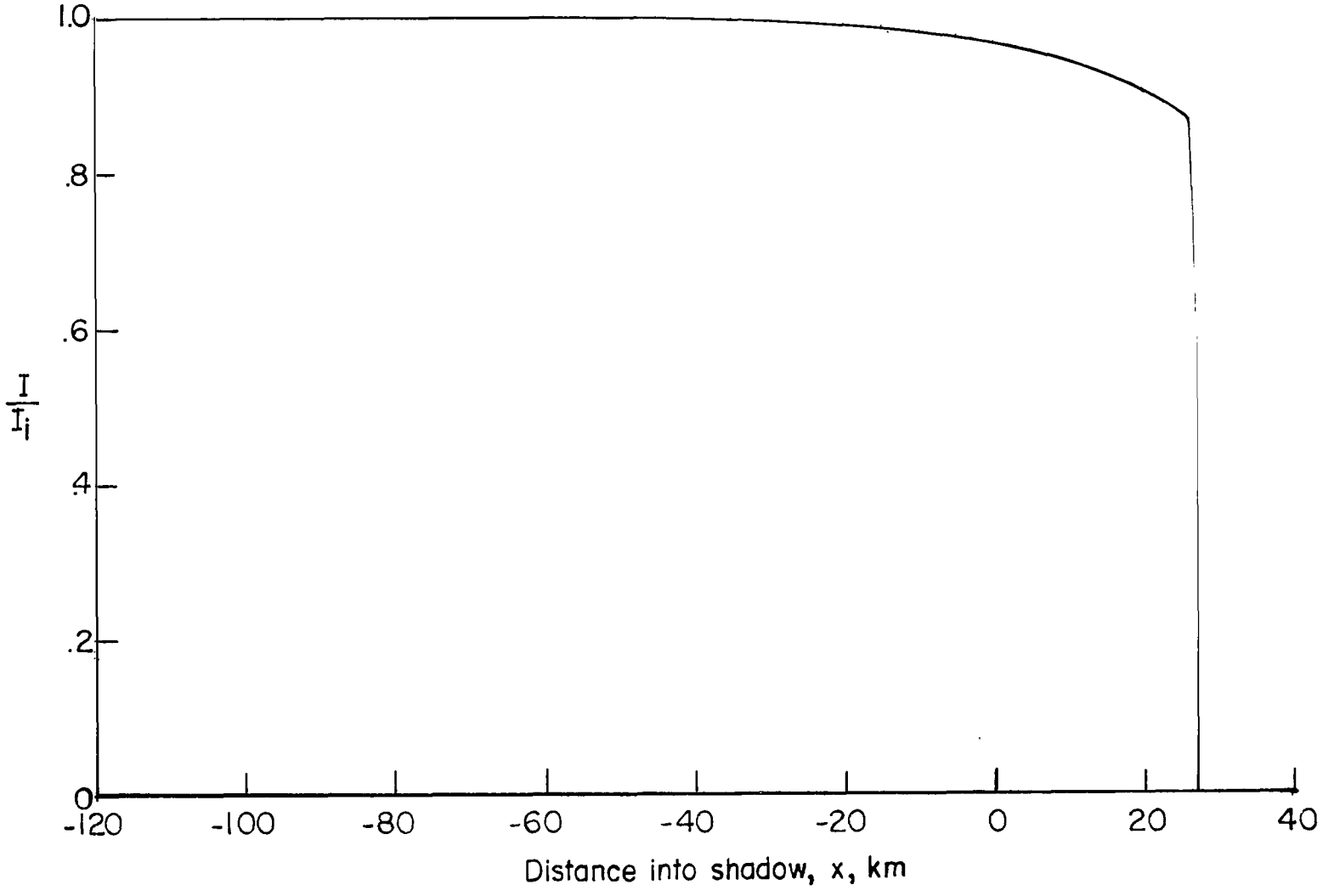

(b) Model II; D = 8700 km.

Figure 4.- Continued.

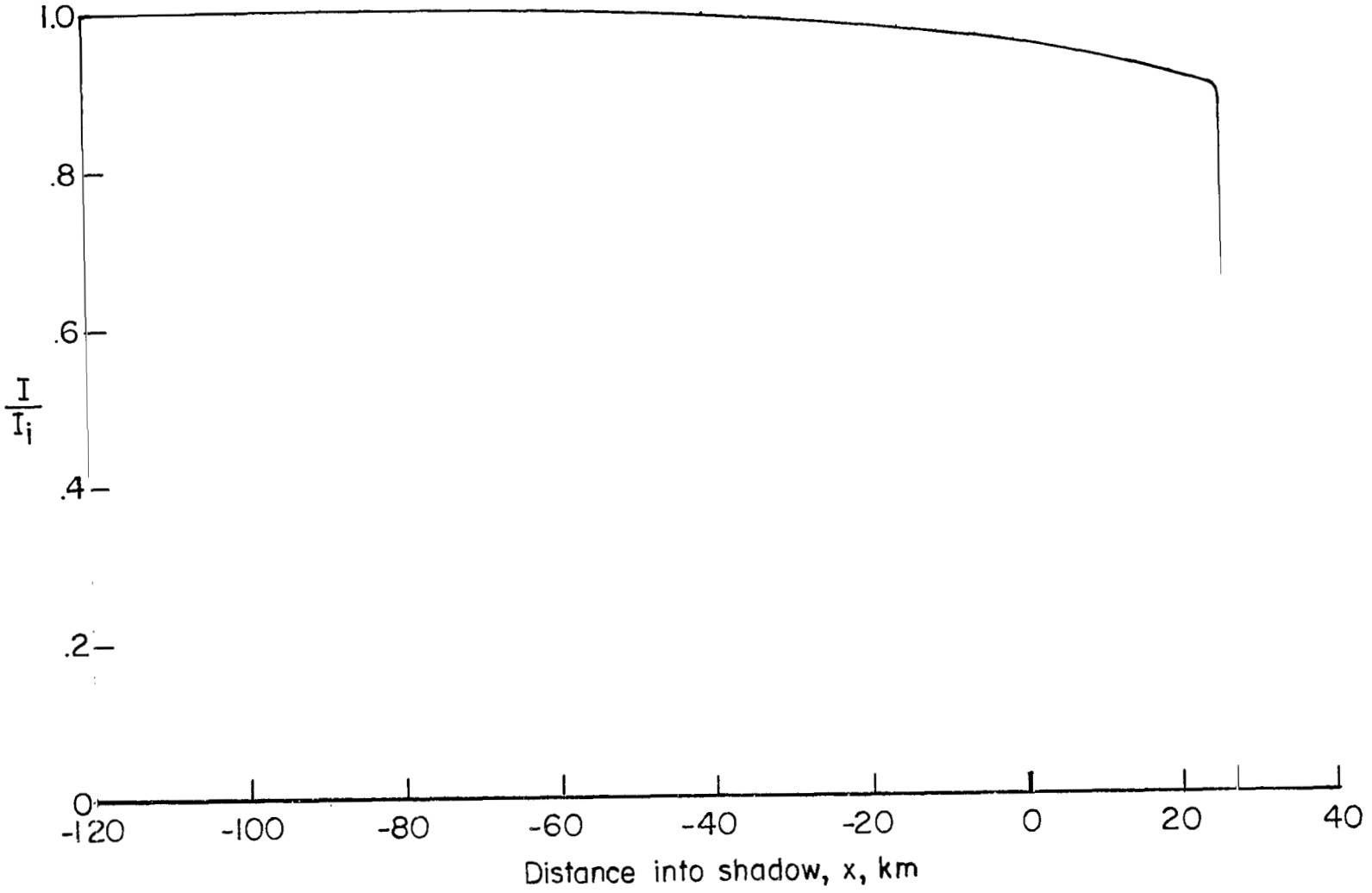

(c) Model III; D = 8700 km.

Figure 4.- Continued.

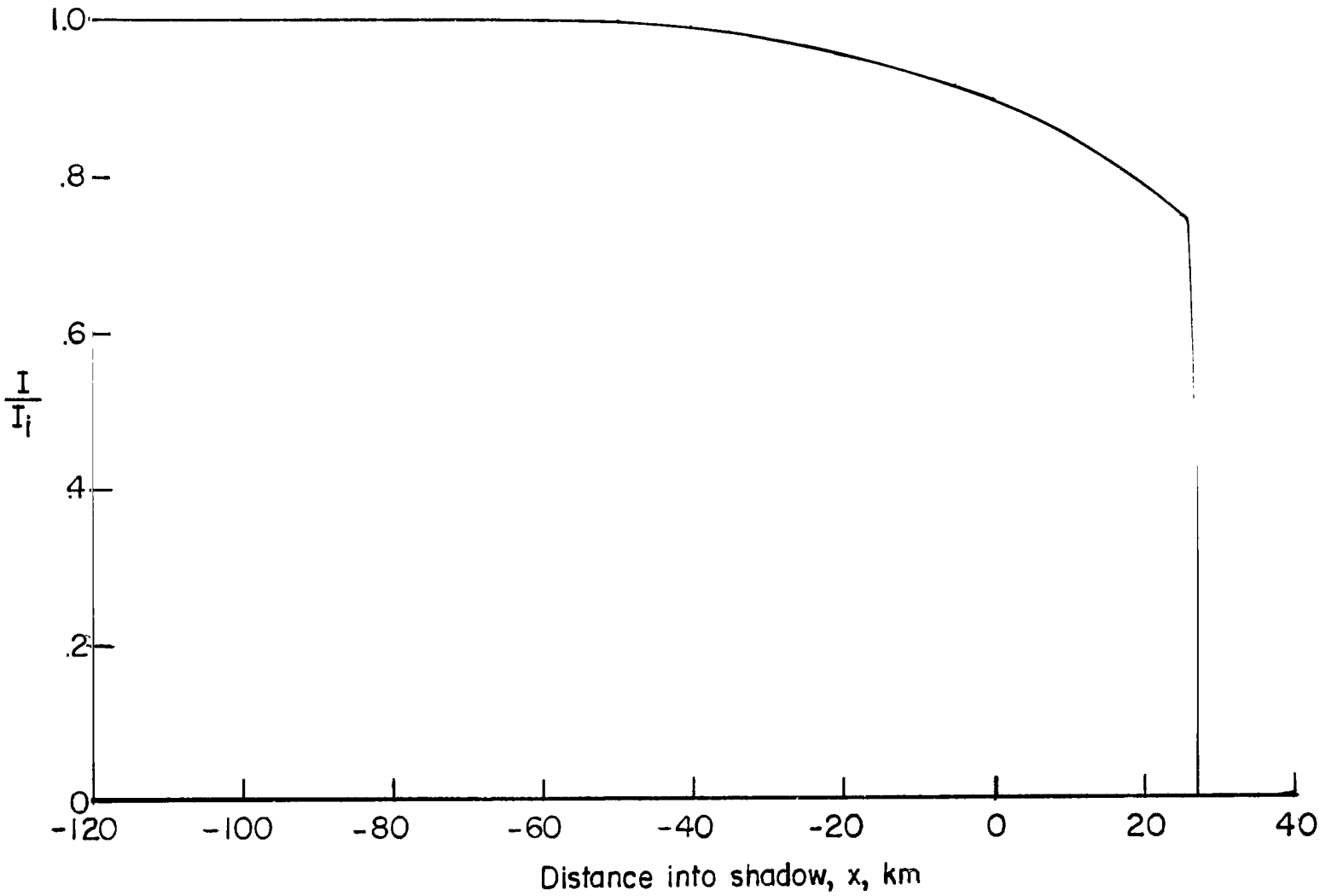

(d) Model IV; D = 8700 km.

Figure 4.- Continued.

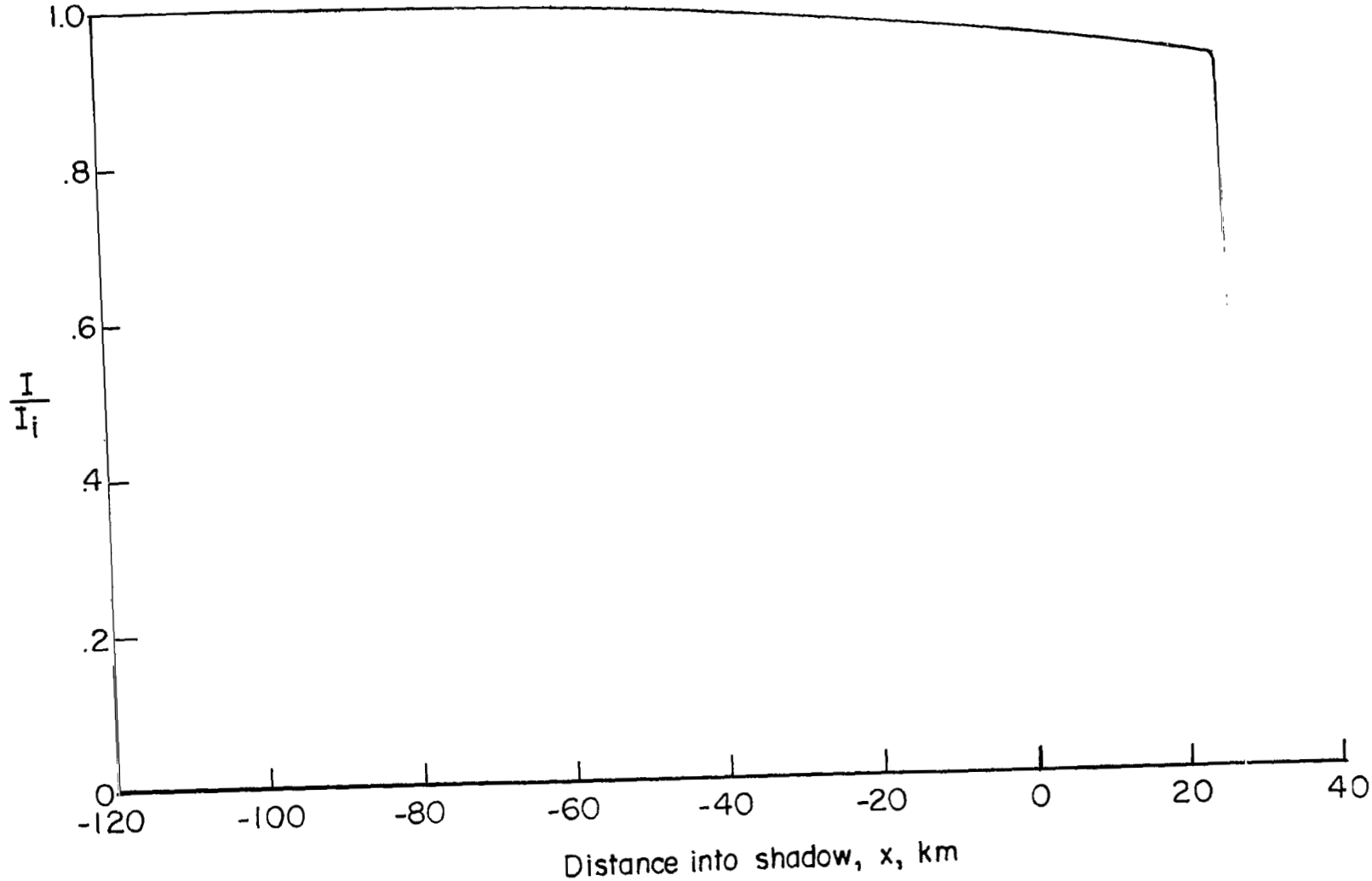

(e) Model V; D = 8700 km.

Figure 4.- Concluded.

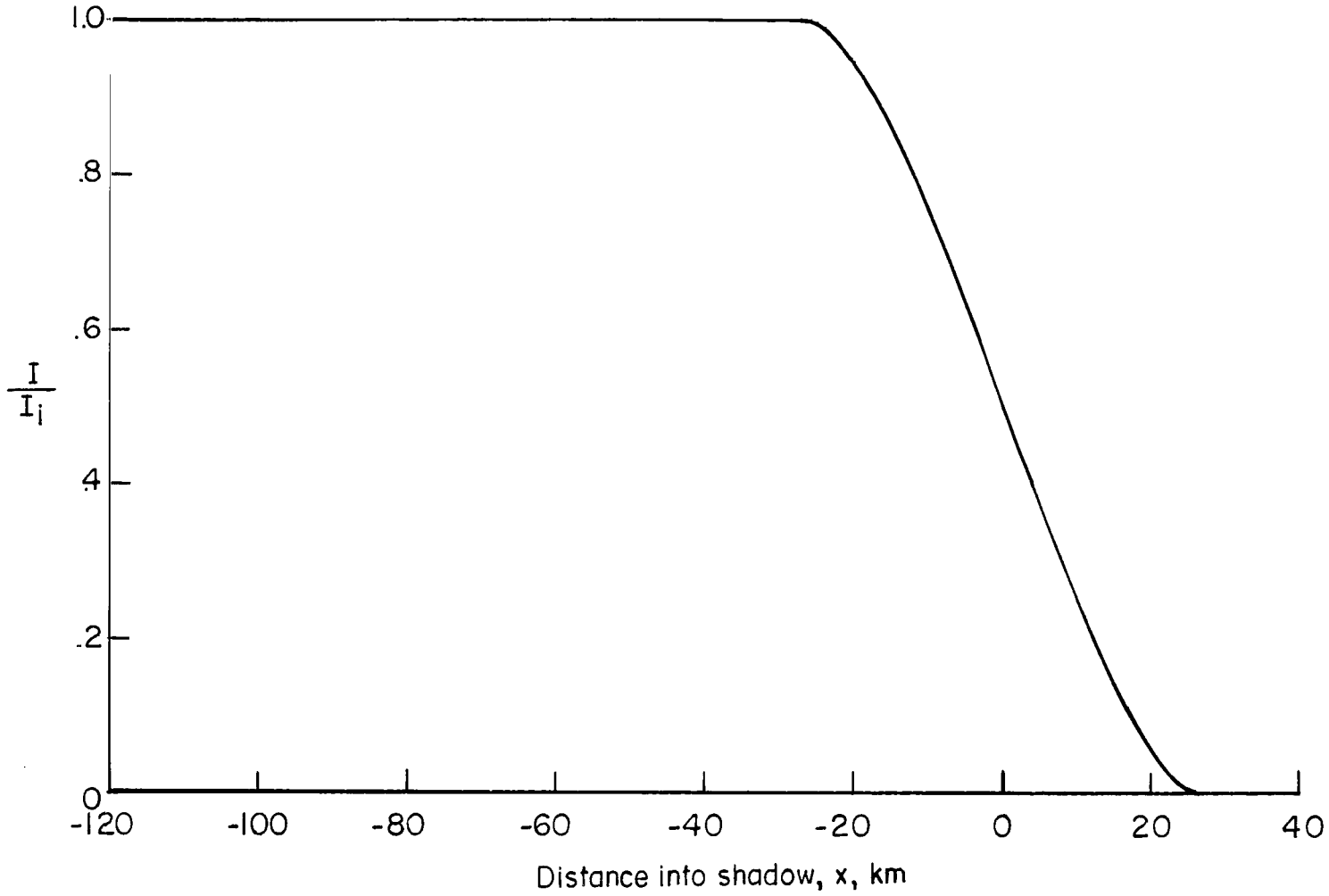

Figure 5.- Light intensity variation for limb darkening and finite size of the sun. D = 8700 km; no atmosphere.

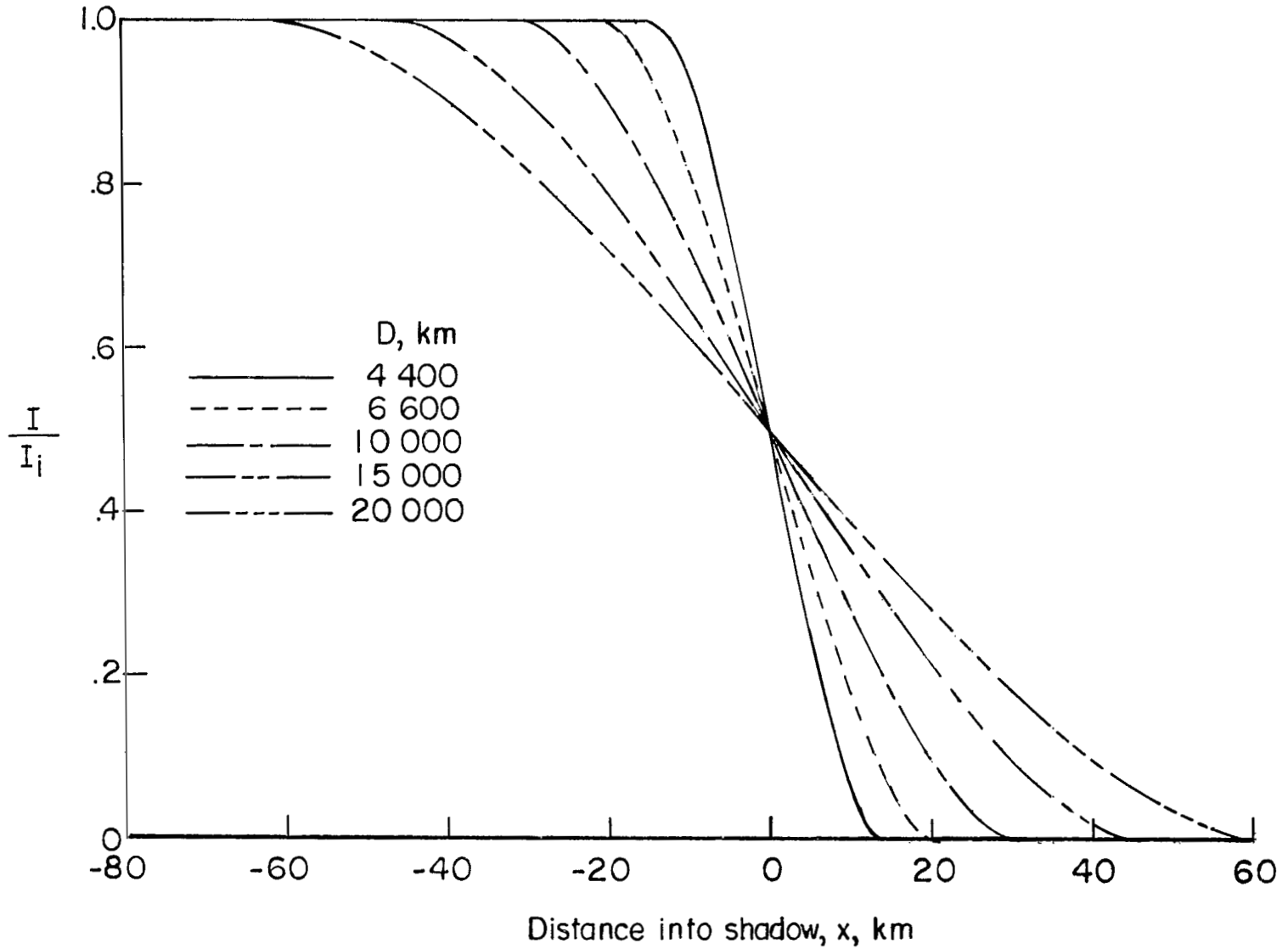

Figure 6.- Finite size and limb darkening effect for a satellite over a range of distances from the planet.

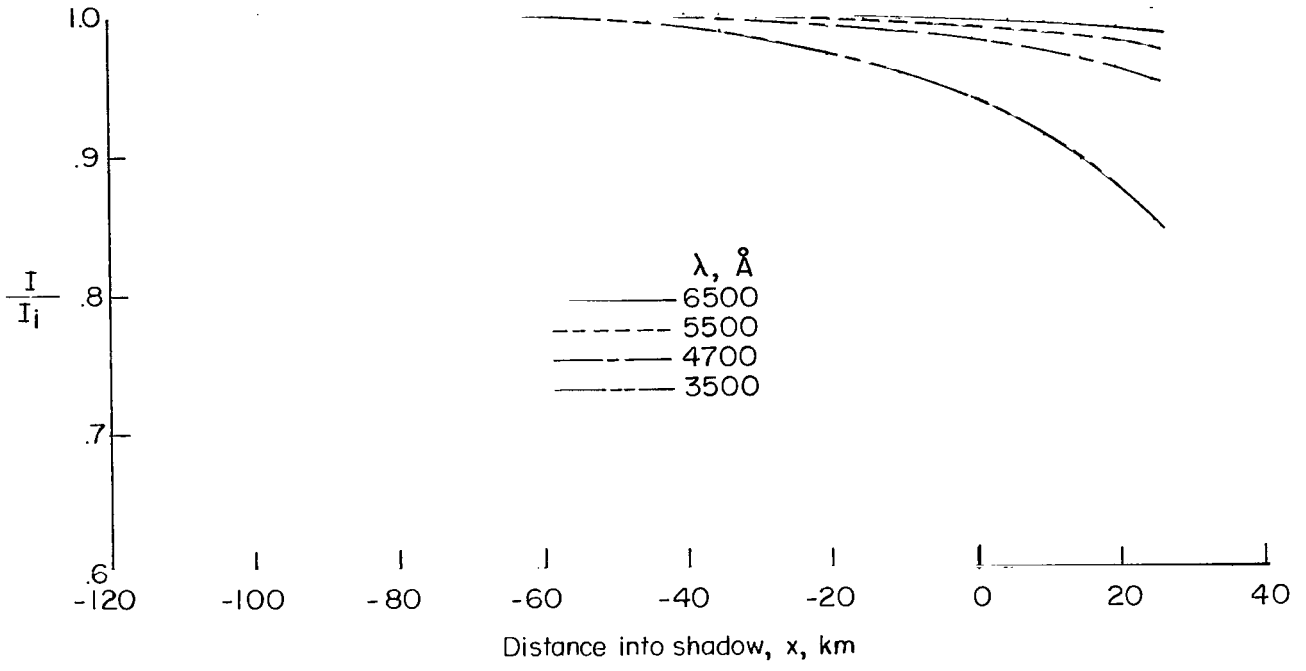

(a) Model I; D = 8700 km.

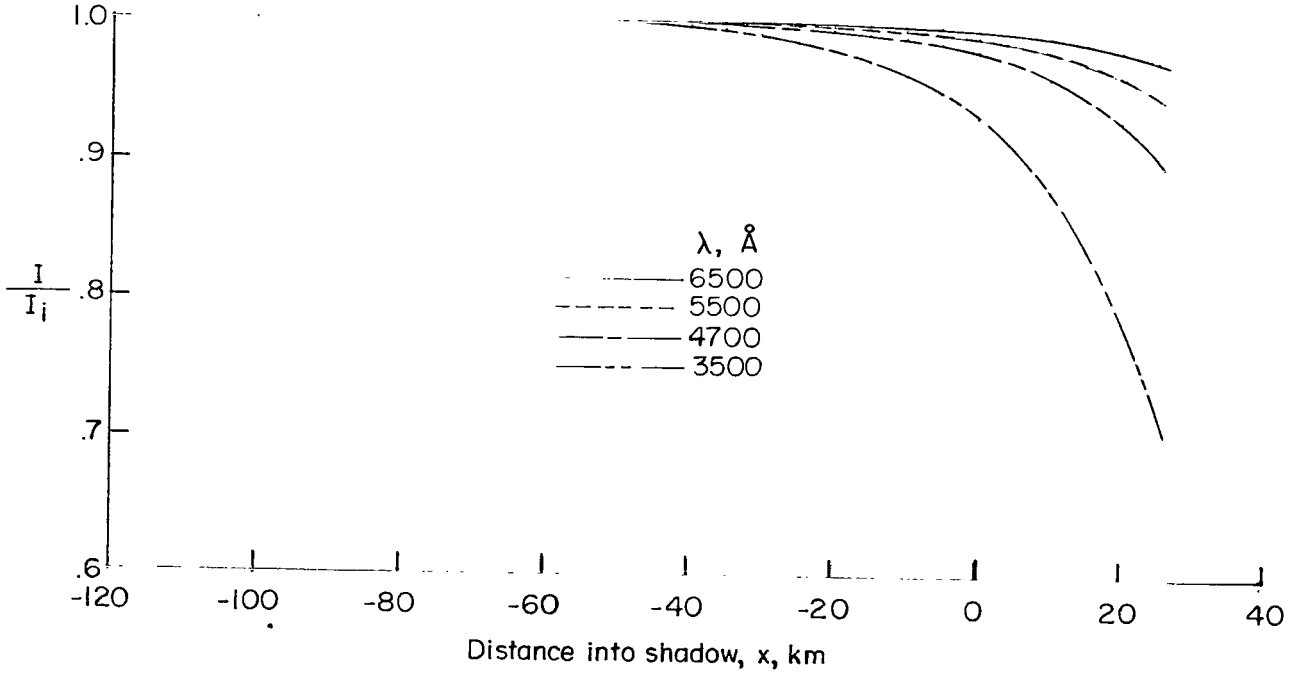

(b) Model II; D = 8700 km.

Figure 7.- The effect of Rayleigh scattering.

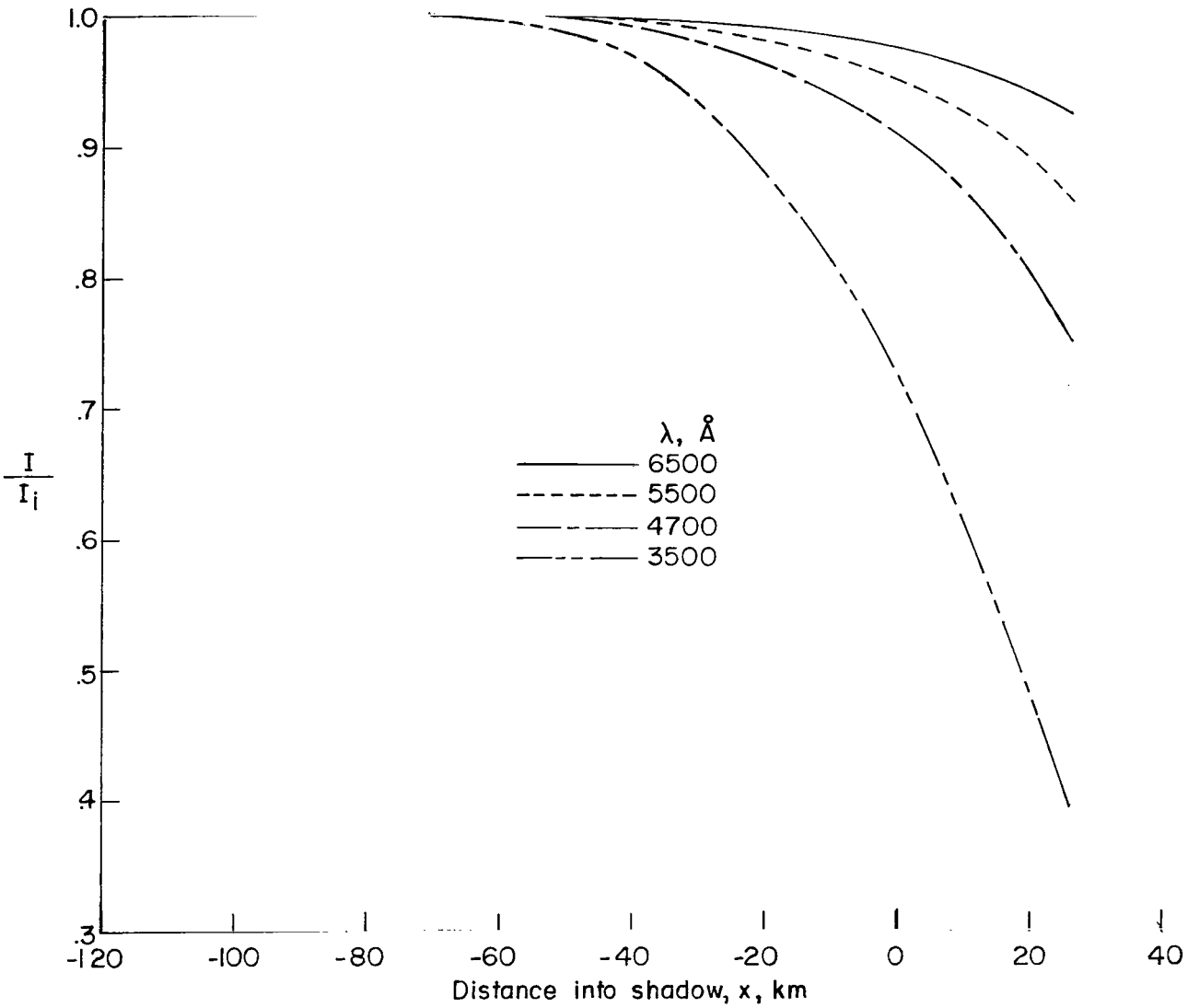

(c) Model III; D = 8700 km.

Figure 7.- Continued.

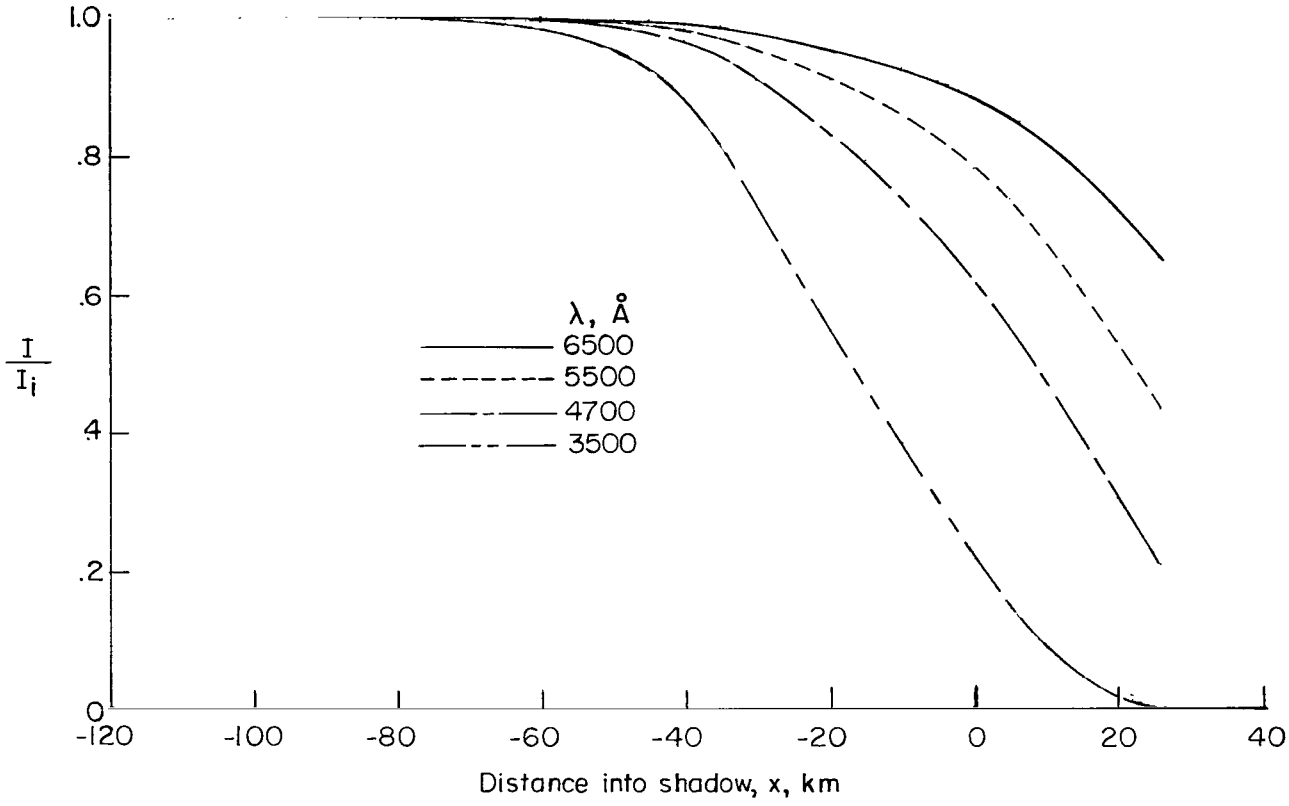

(d) Model IV; D = 8700 km.

Figure 7.- Continued.

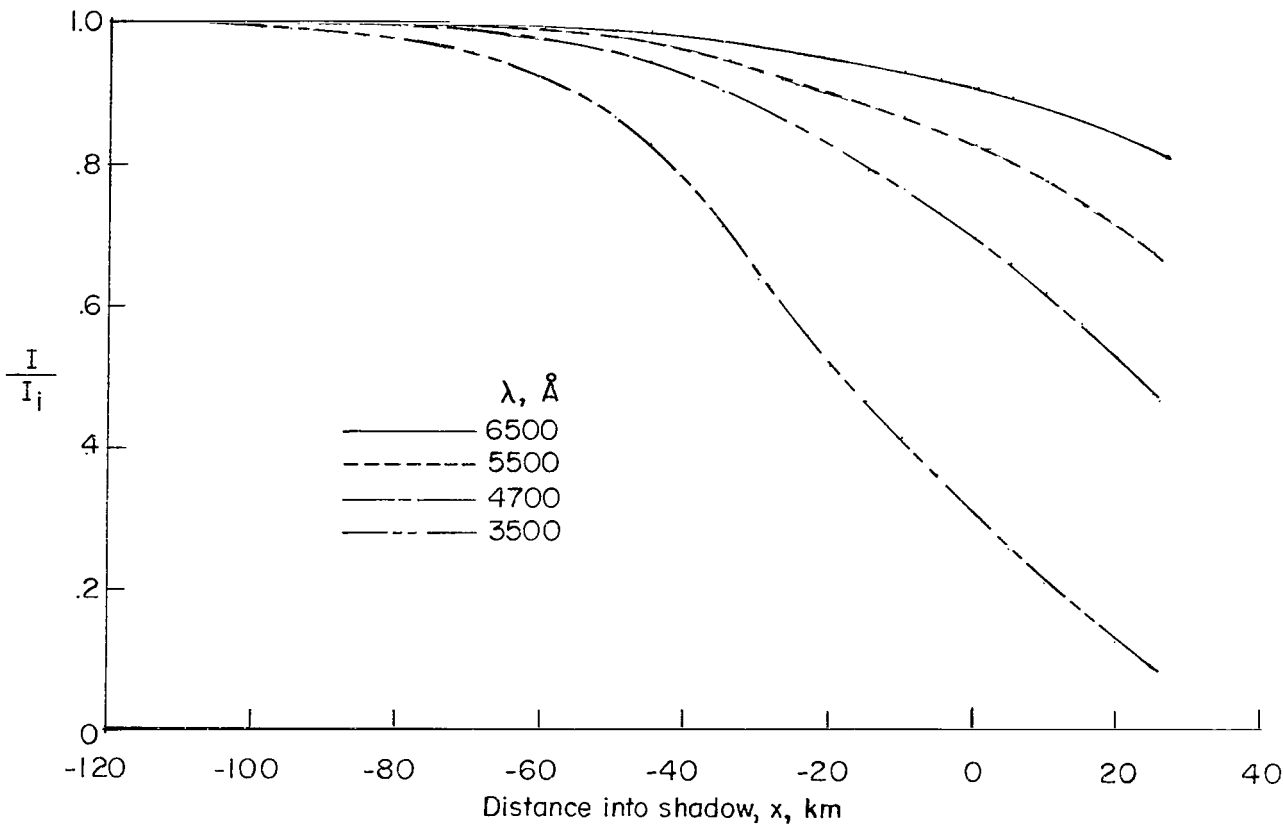

(e) Model V; D = 8700 km.

Figure 7.- Concluded.

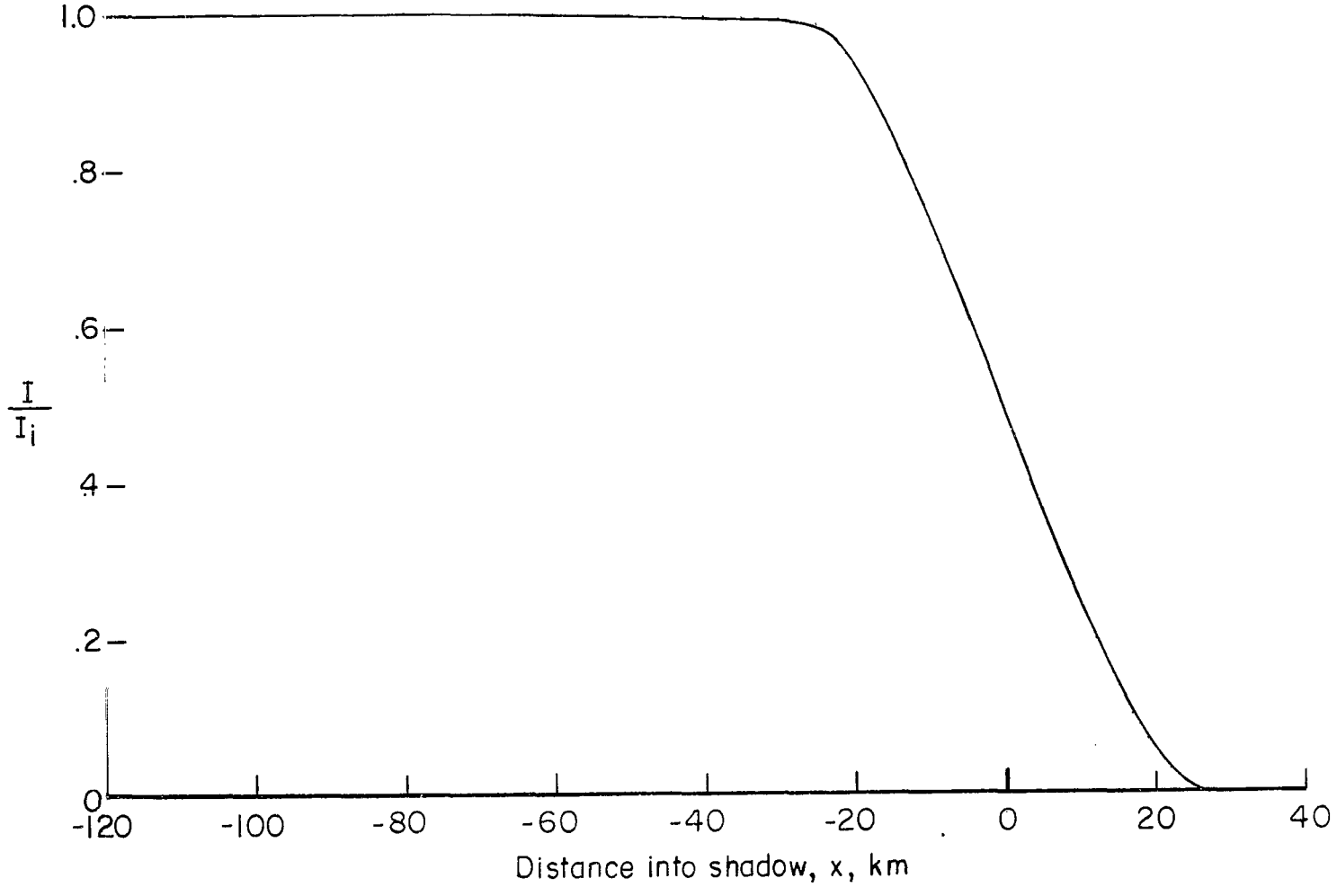

(a) Model I; D = 8700 km.

Figure 8.- Combined effects for λ = 6500 angstroms.

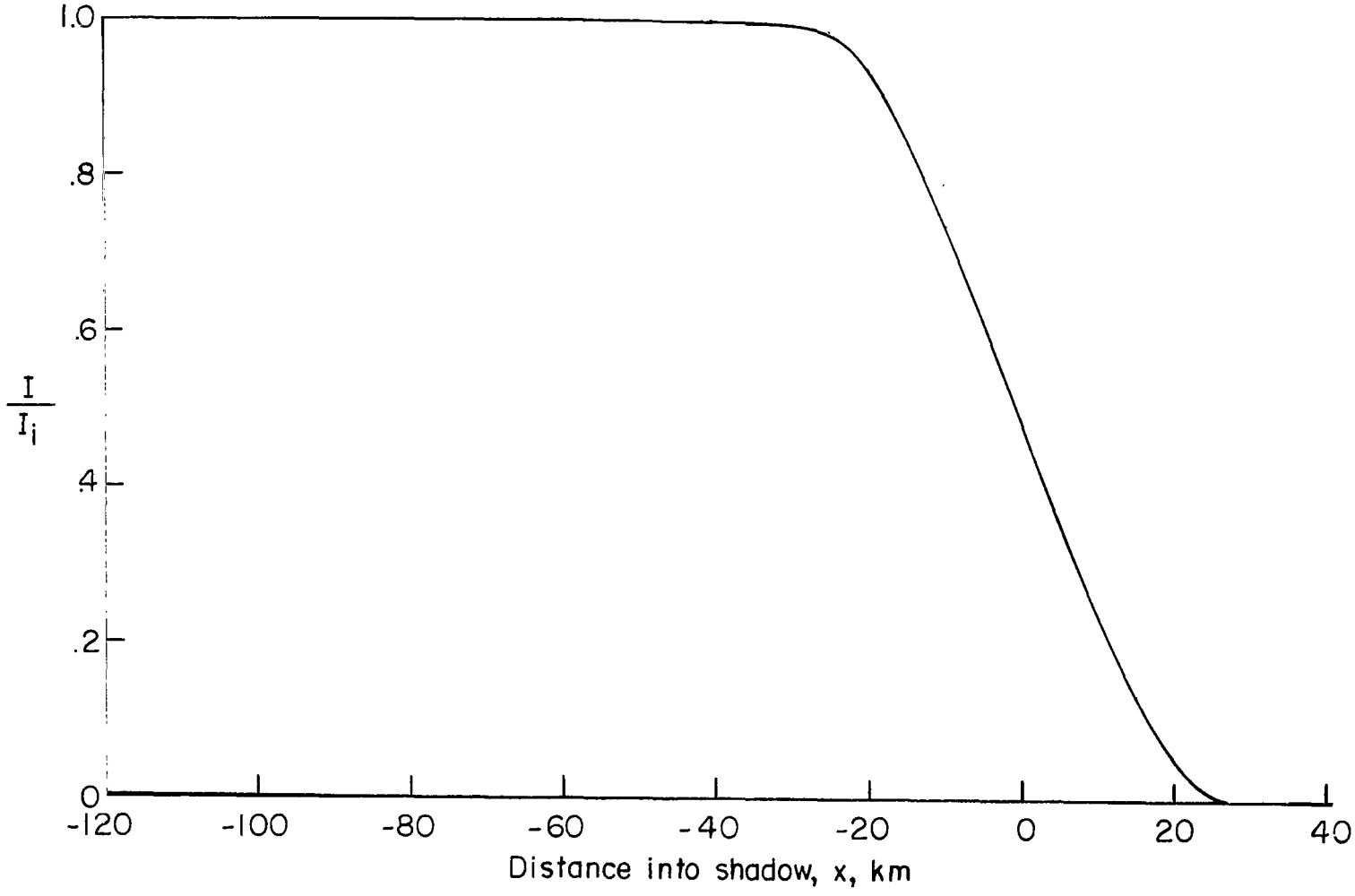

(b) Model II; D = 8700 km.

Figure 8.- Continued.

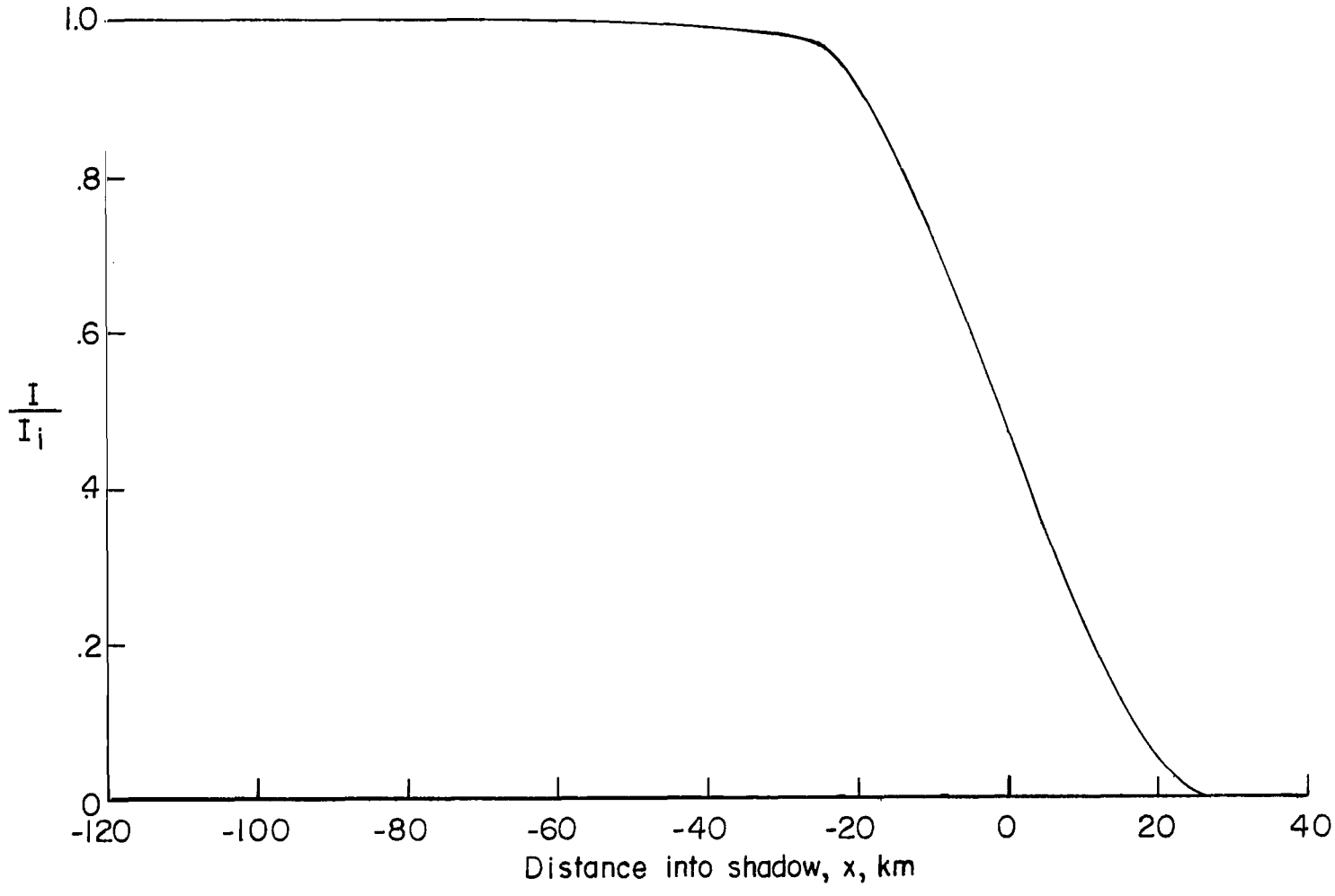

(c) Model III; D = 8700 km.

Figure 8.- Continued.

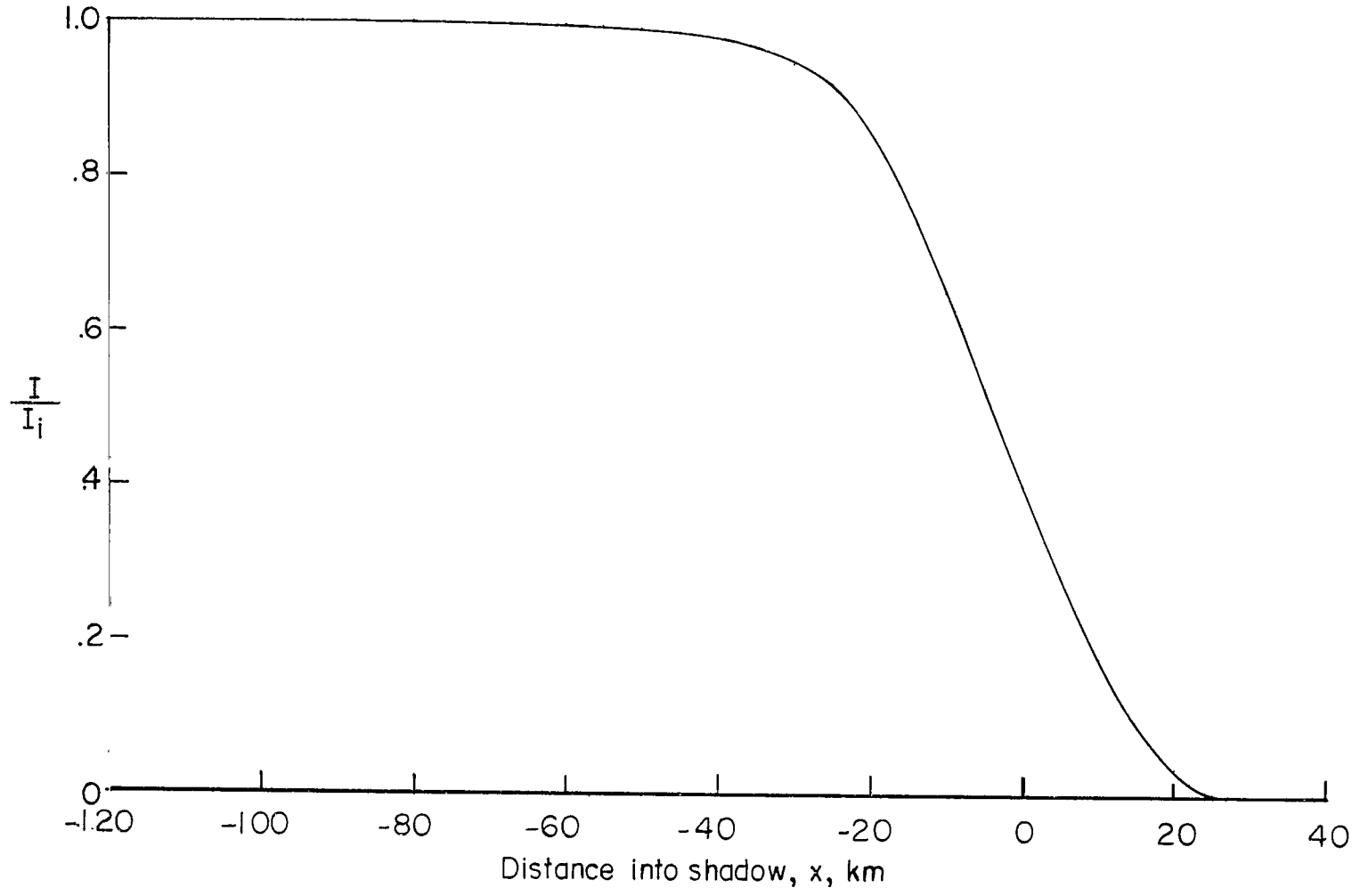

(d) Model IV; D = 8700 km.

Figure 8.- Continued.

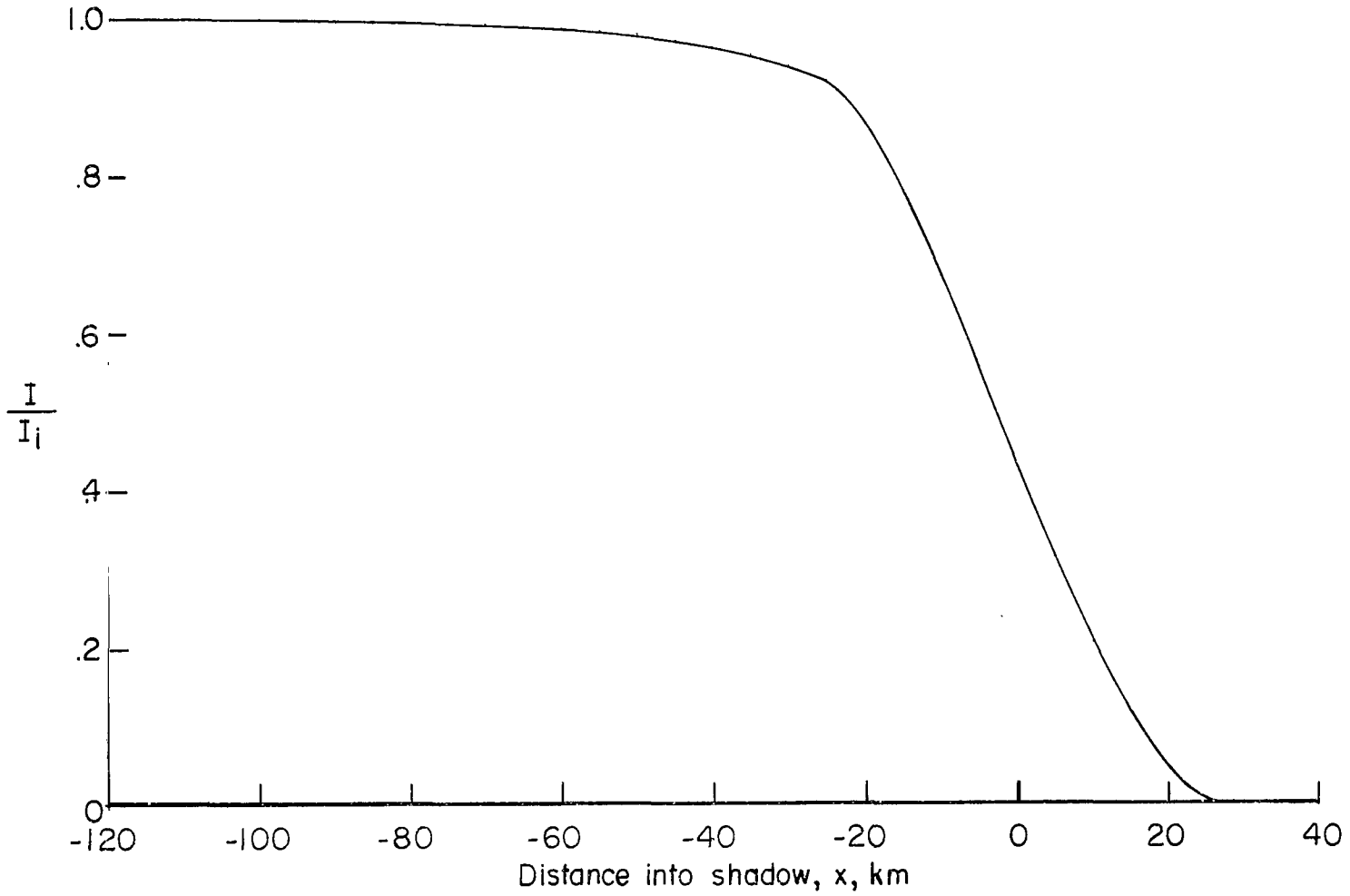

(e) Model V; D = 8700 km.

Figure 8.- Concluded.

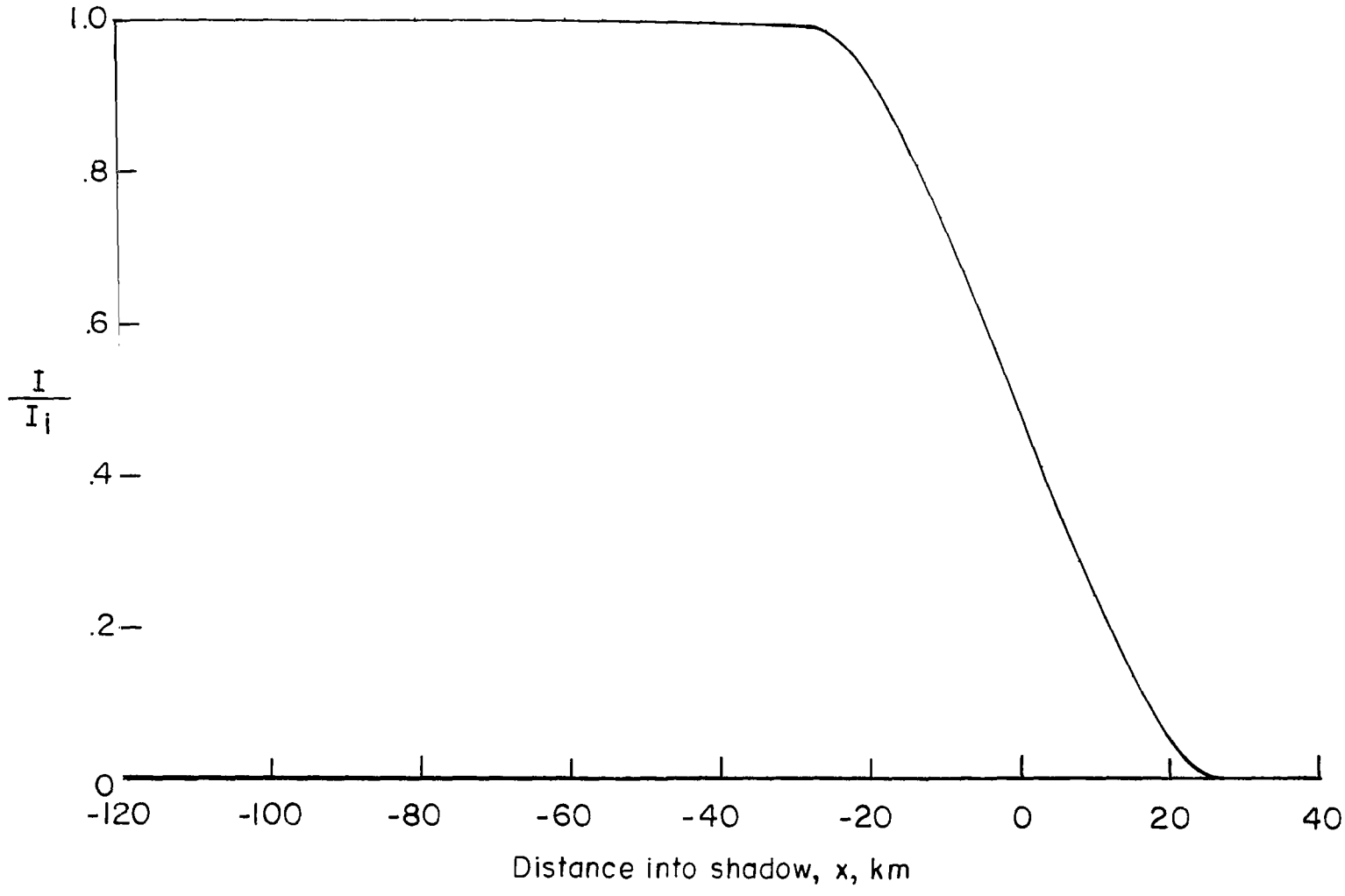

(a) Model I; D = 8700 km.

Figure 9.- Combined effects for λ = 5500 angstroms.

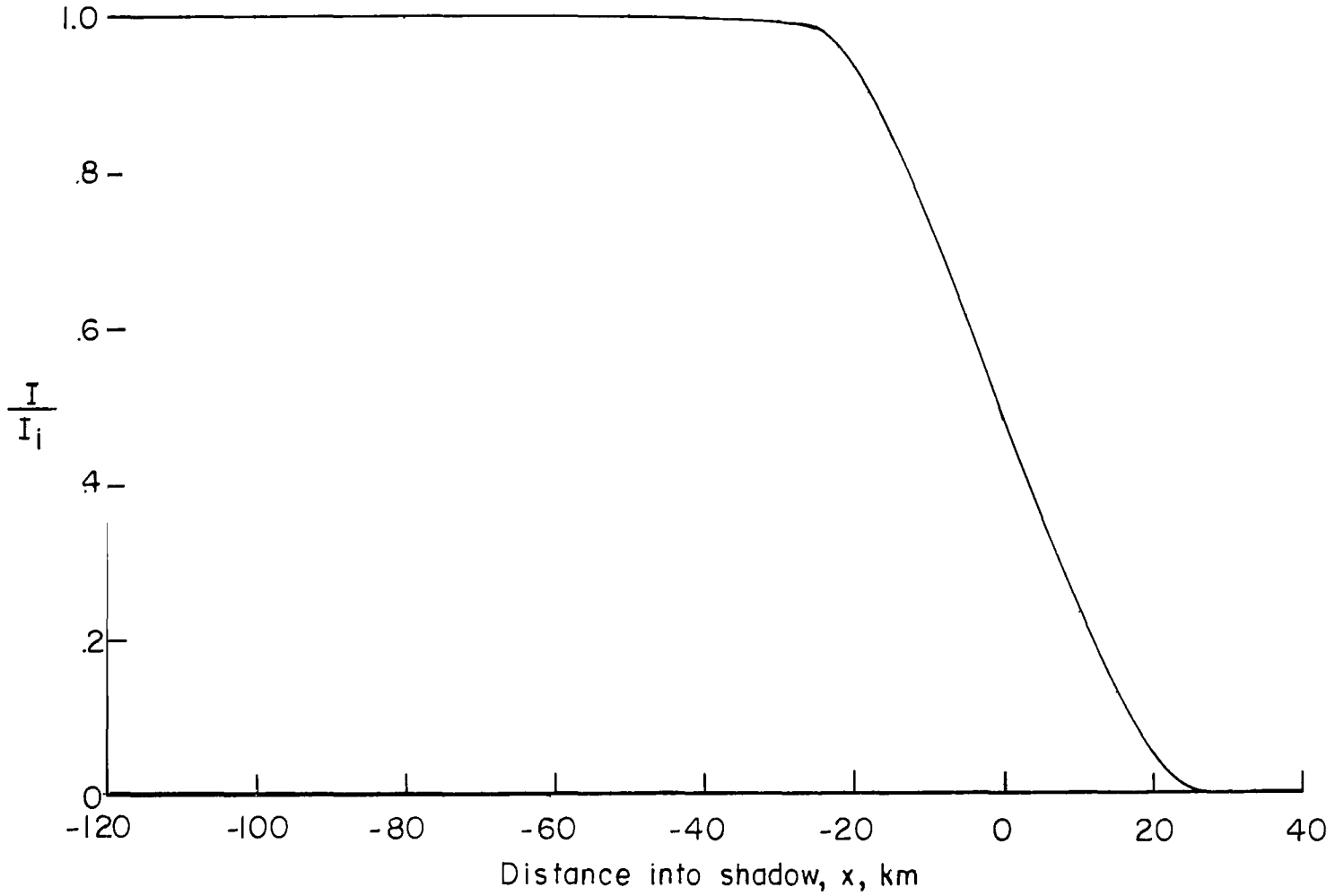

(b) Model II; D = 8700 km.

Figure 9.- Continued.

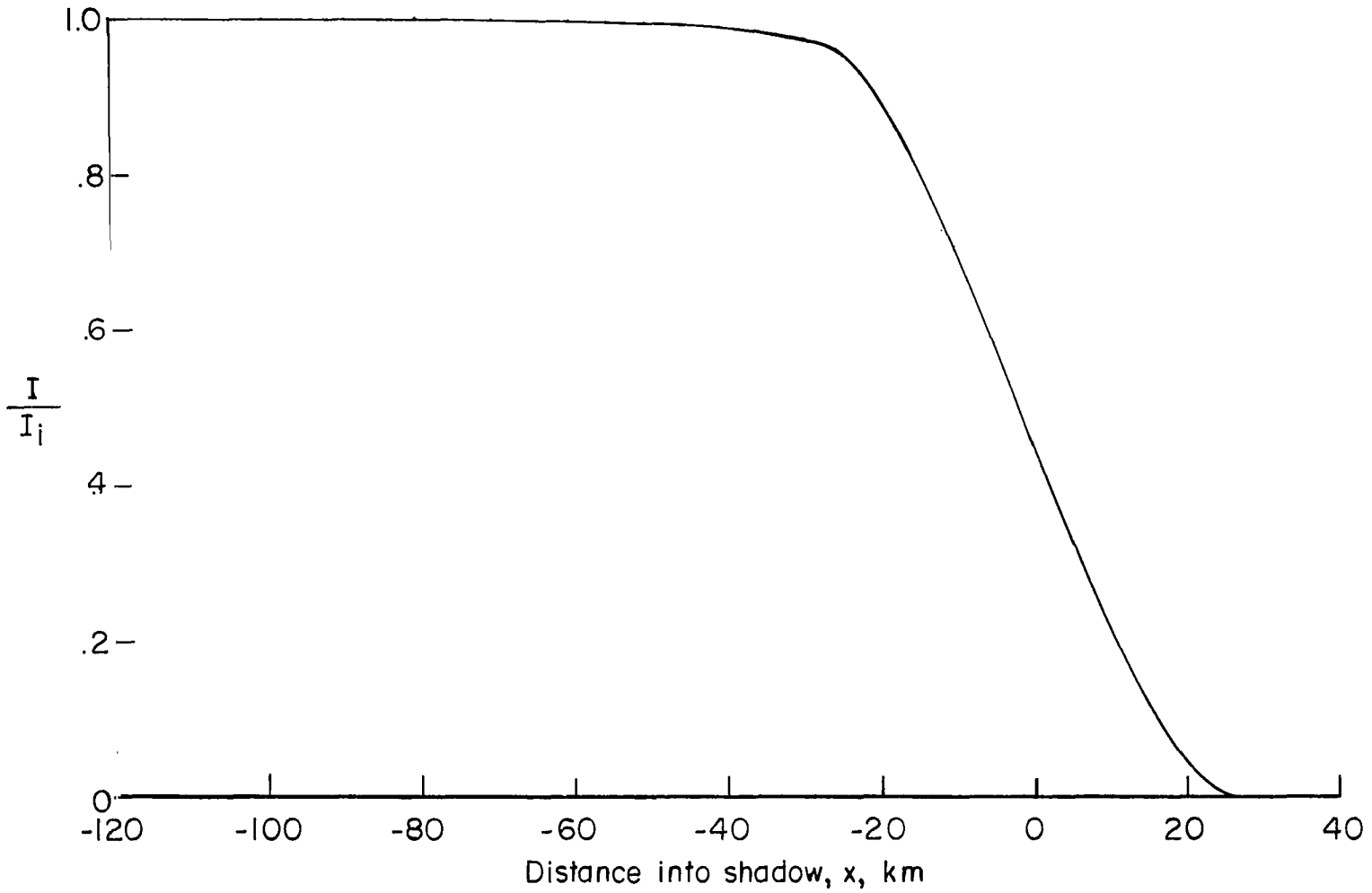

(c) Model III; D = 8700 km.

Figure 9.- Continued.

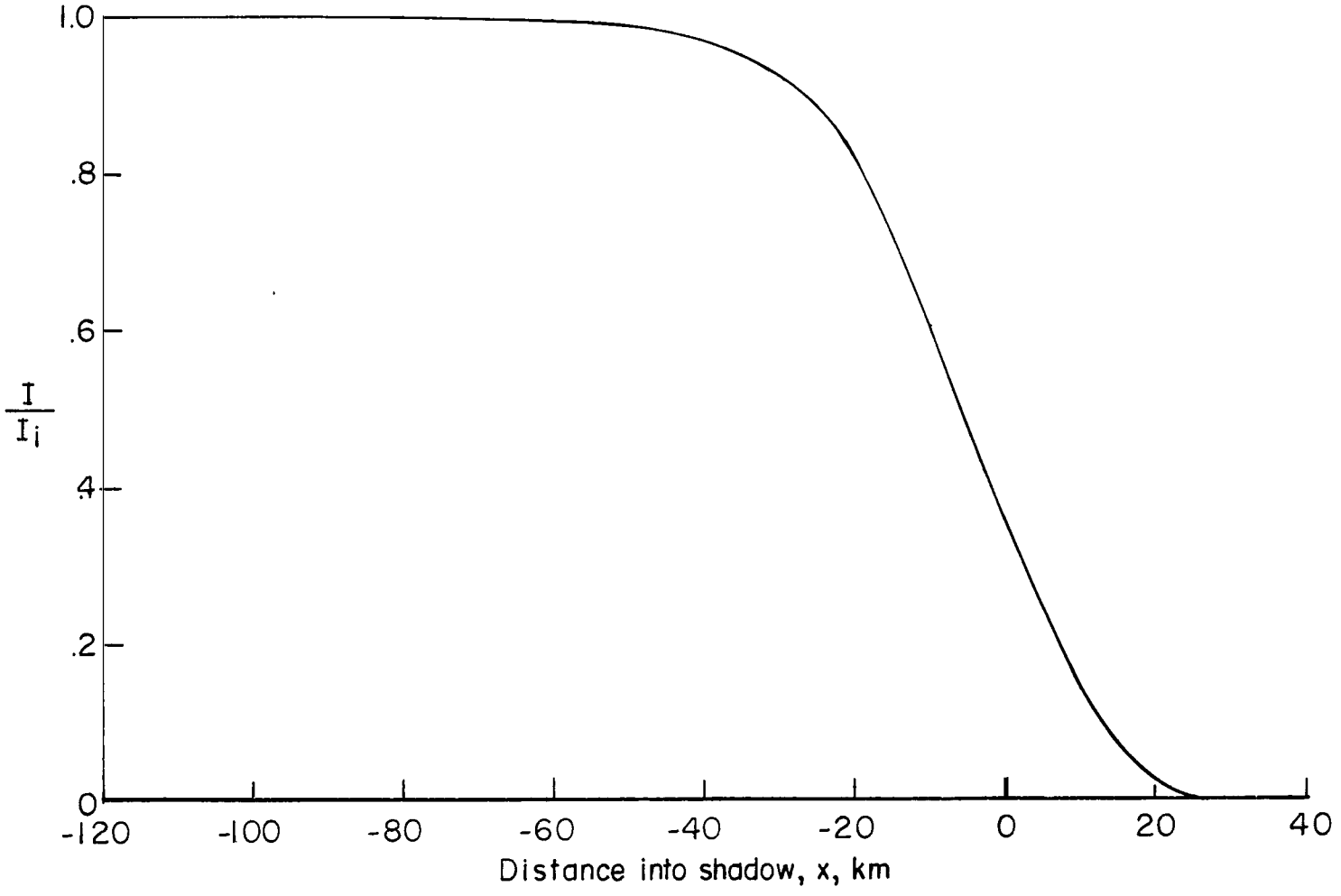

(d) Model IV; D = 8700 km.

Figure 9.- Continued.

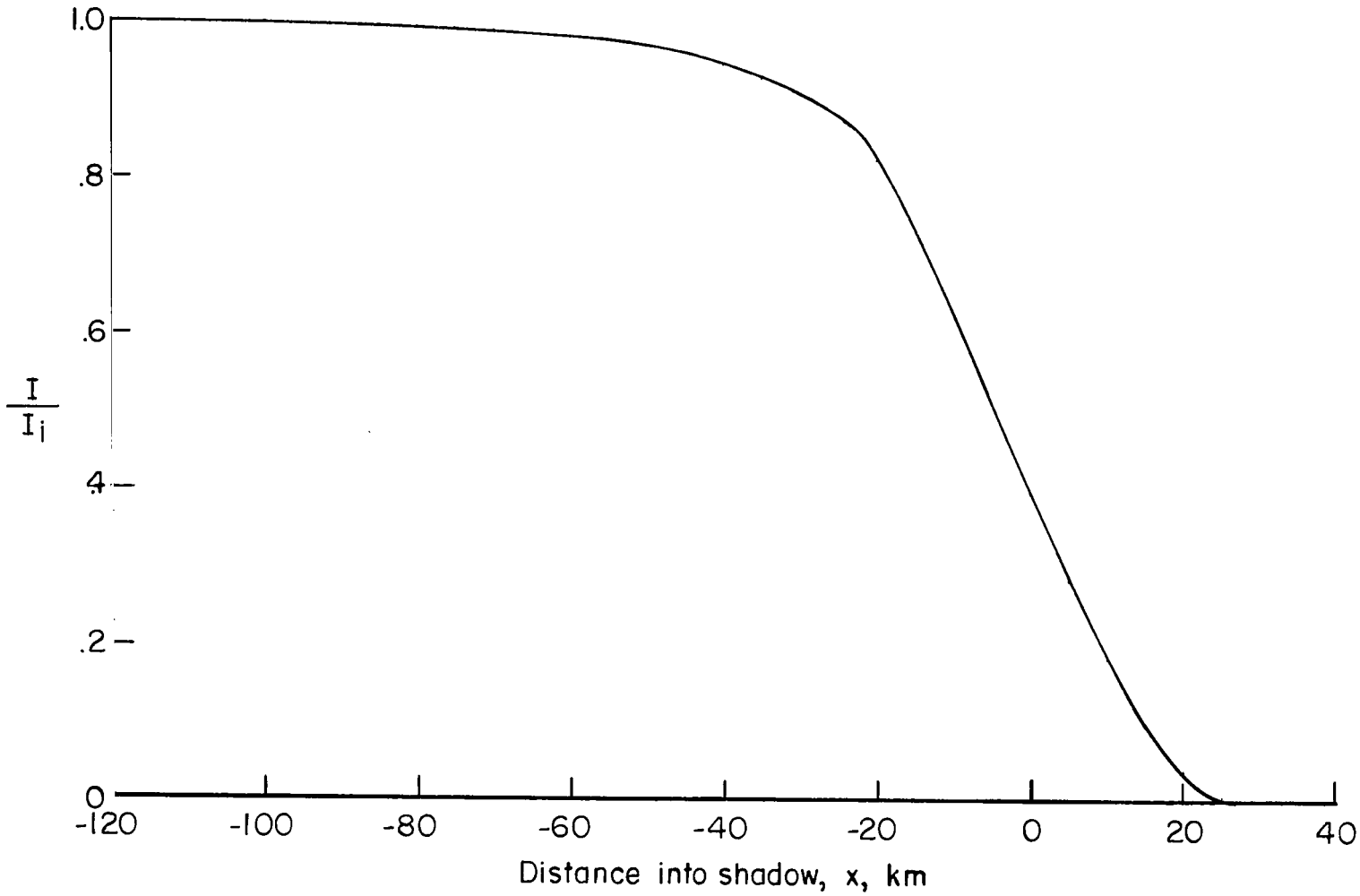

(e) Model V; D = 8700 km.

Figure 9.- Concluded.

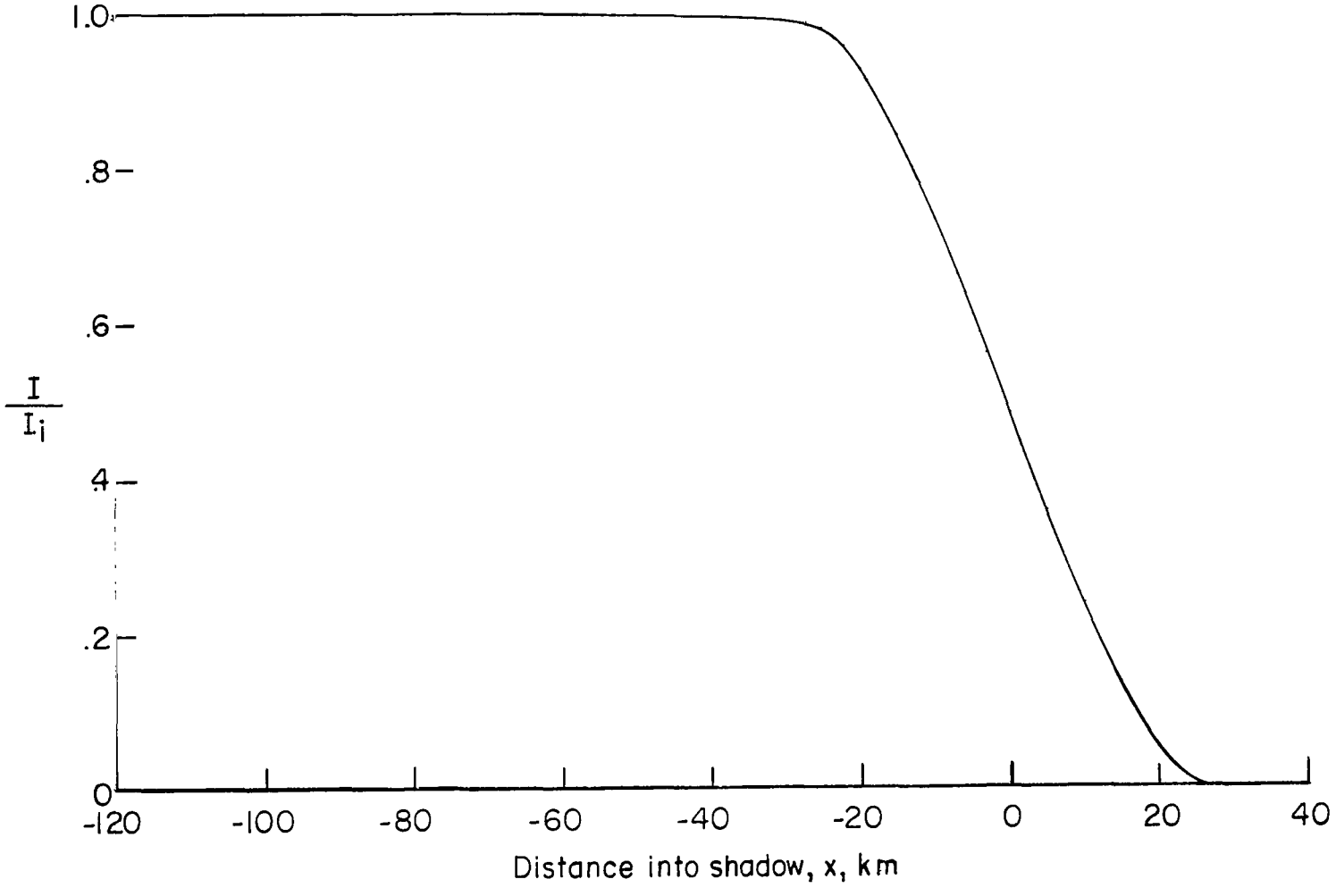

(a) Model I; D = 8700 km.

Figure 10.- Combined effects for λ = 4700 angstroms.

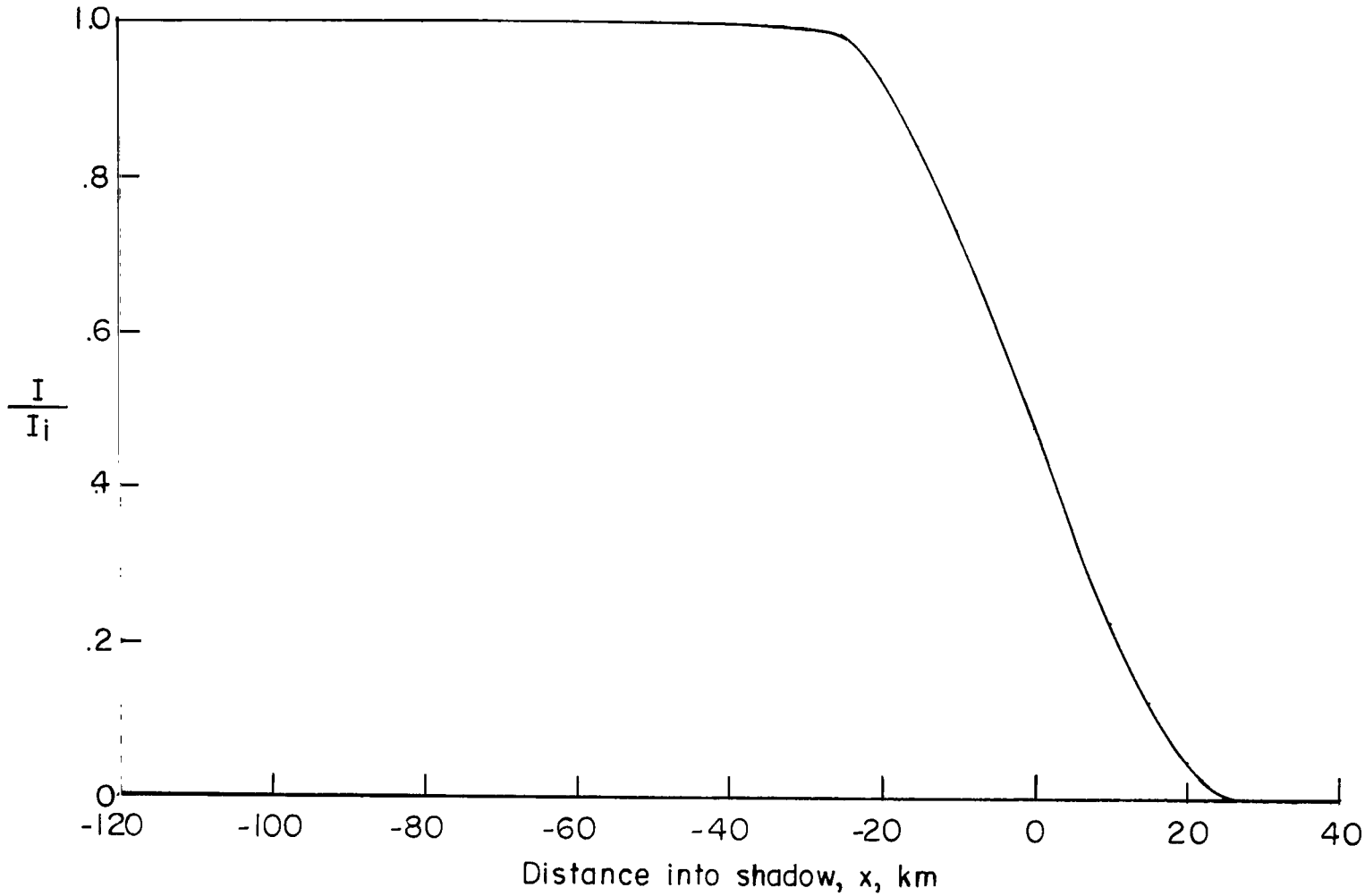

(b) Model II; D = 8700 km.

Figure 10.- Continued.

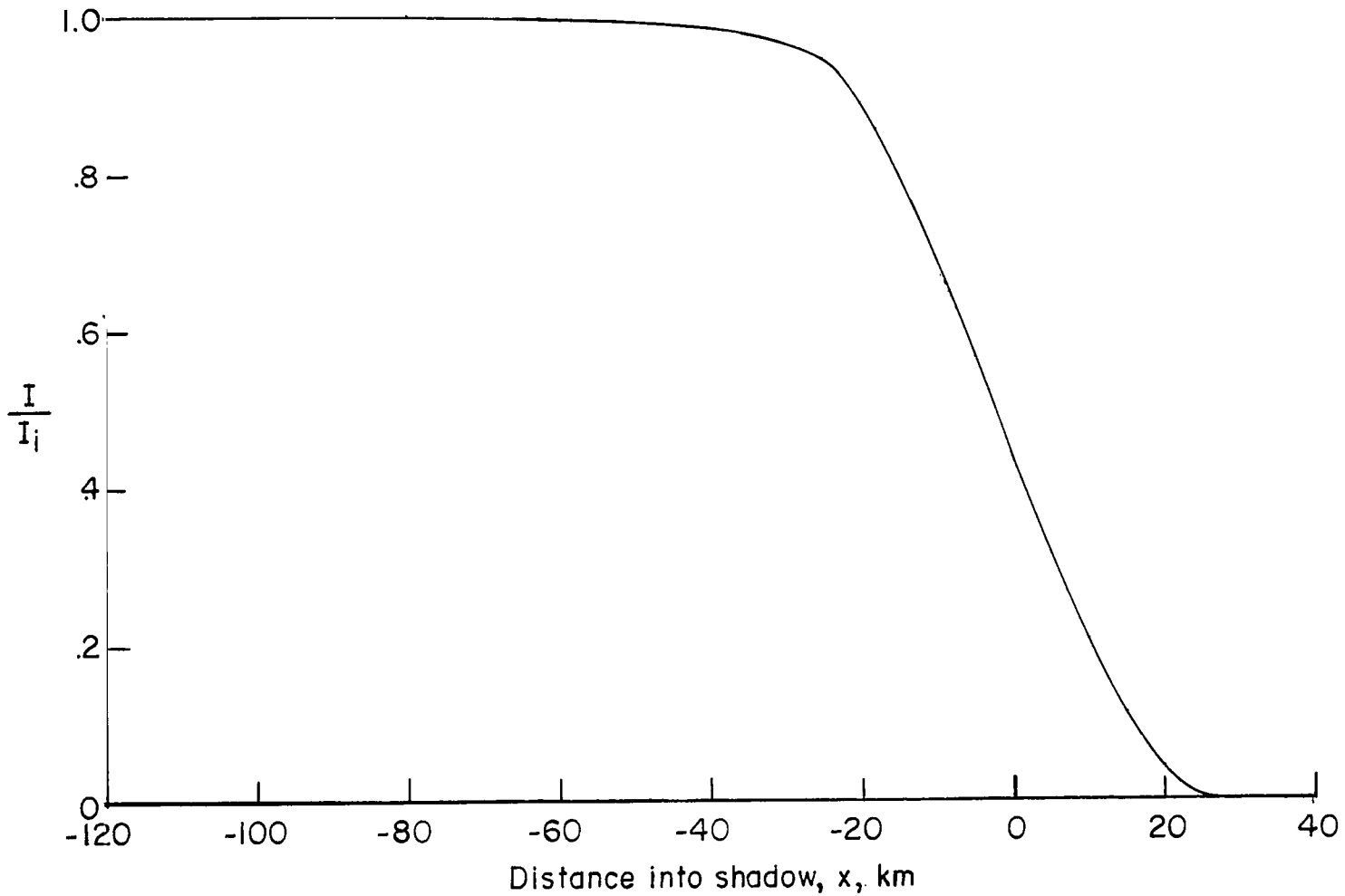

(c) Model III; D = 8700 km.

Figure 10.- Continued.

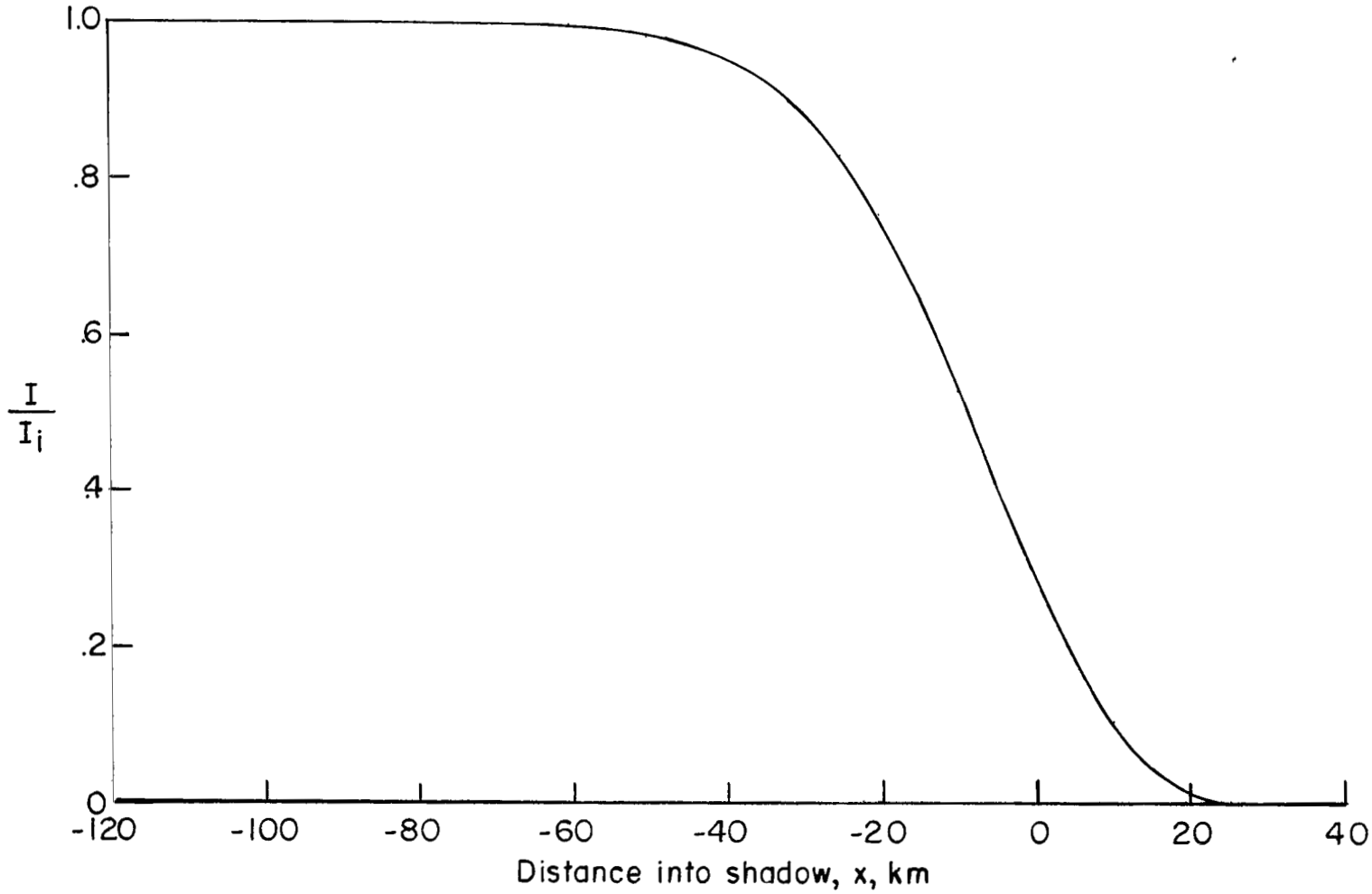

(d) Model IV; D = 8700 km.

Figure 10.- Continued.

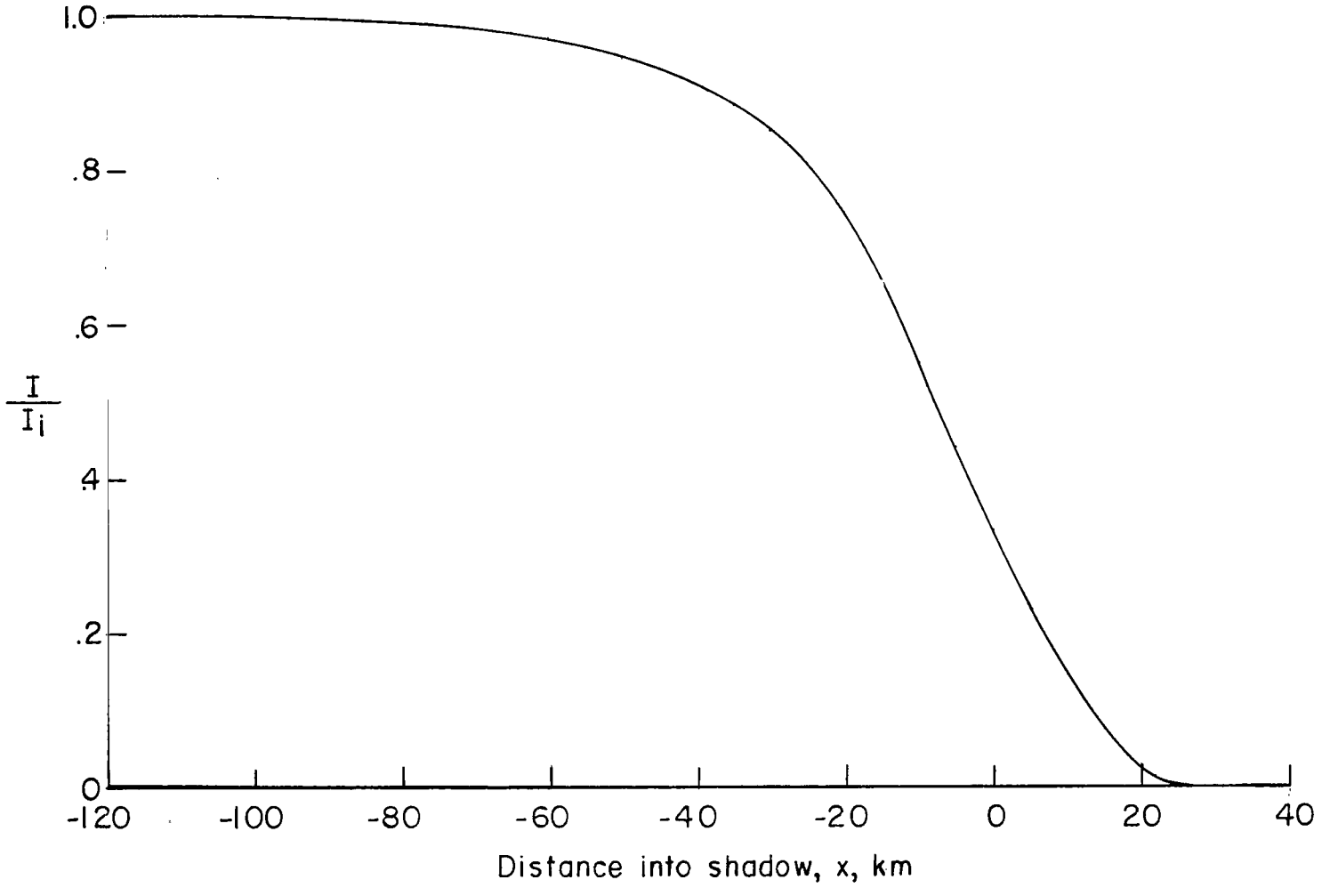

(e) Model V; D = 8700 km.

Figure 10.- Concluded.

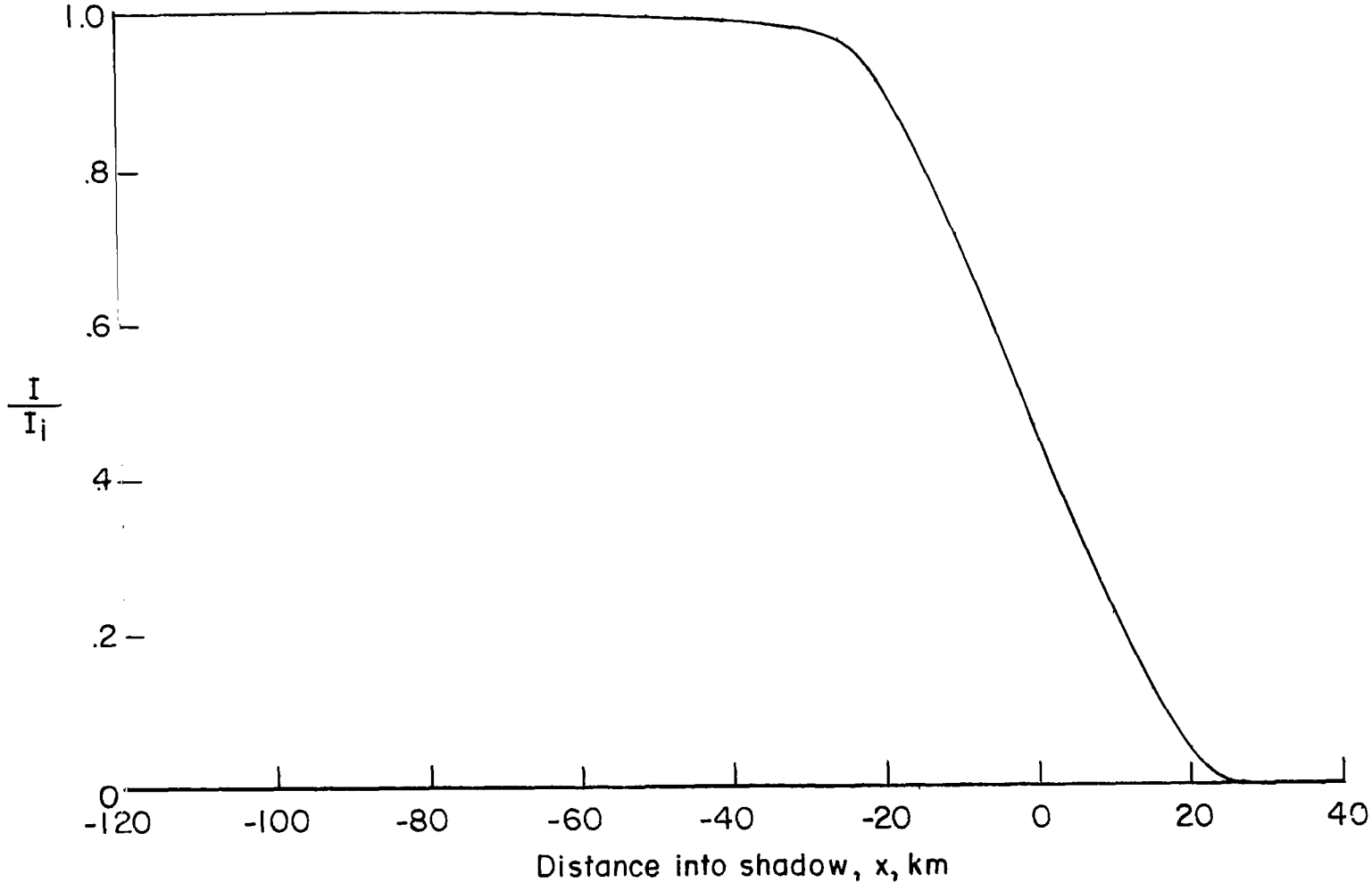

(a) Model I; D = 8700 km.

Figure 11.- Combined effects for λ = 3500 angstroms.

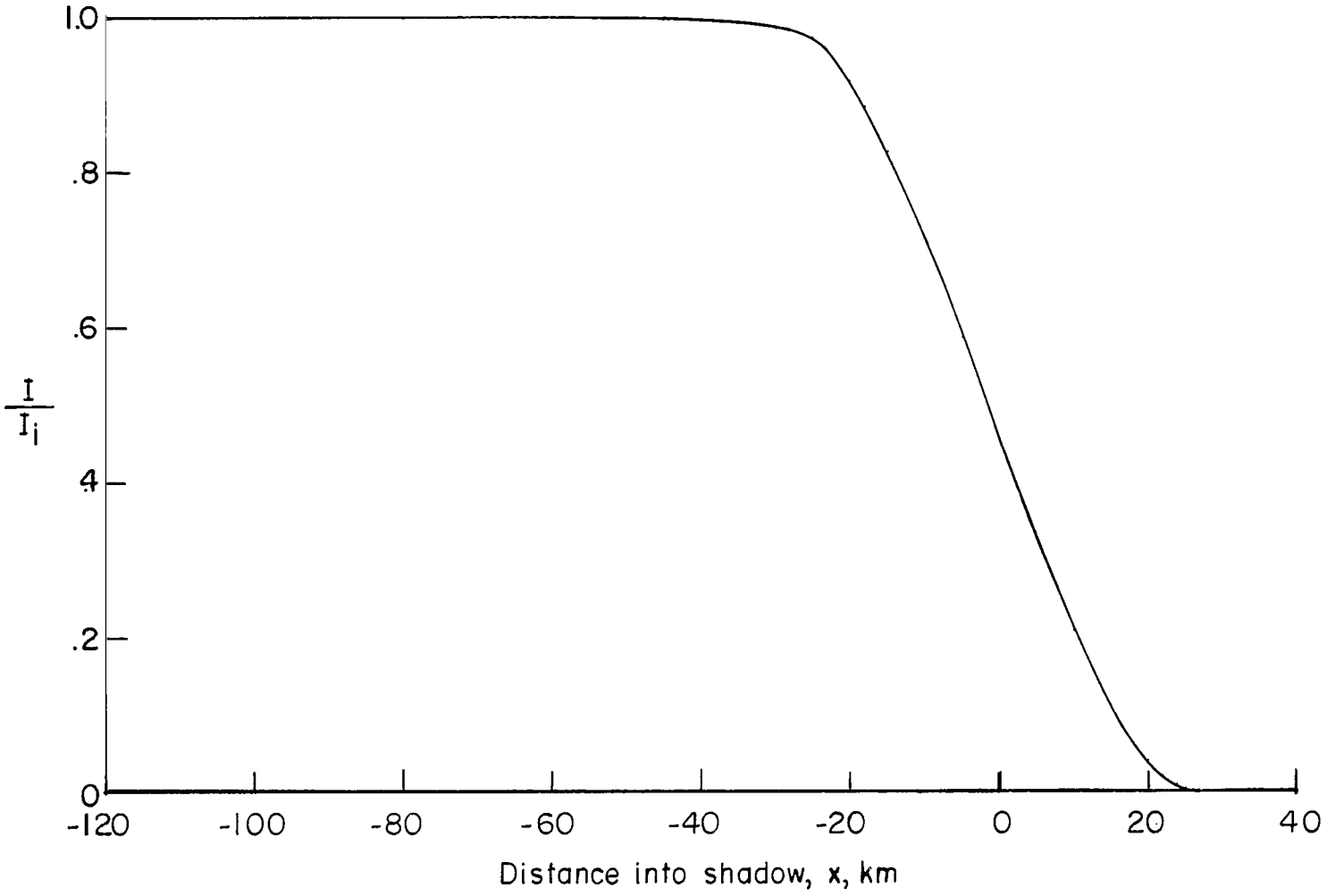

(b) Model II; D = 8700 km.

Figure 11.- Continued.

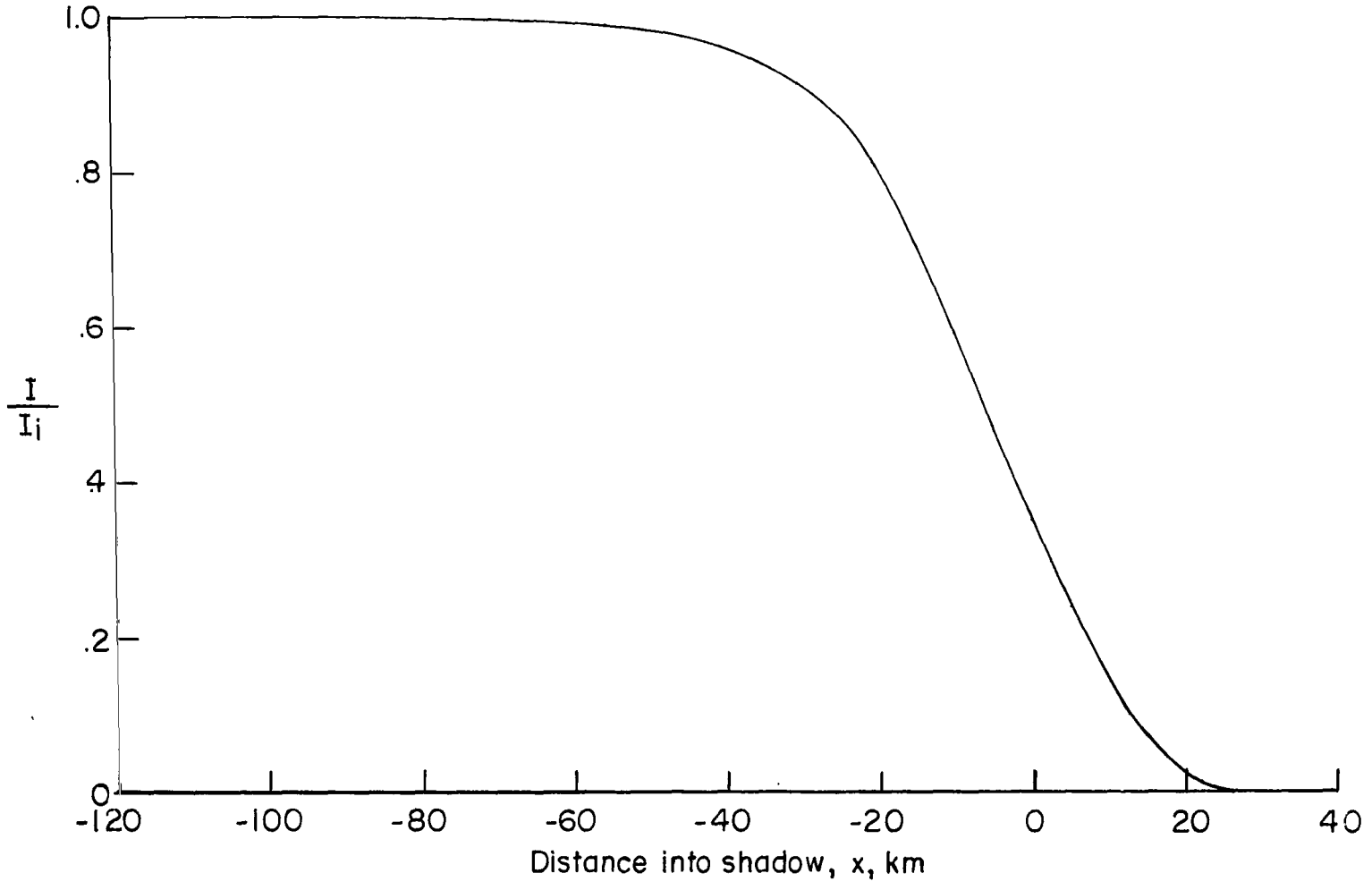

(c) Model III; D = 8700 km.

Figure 11.- Continued.

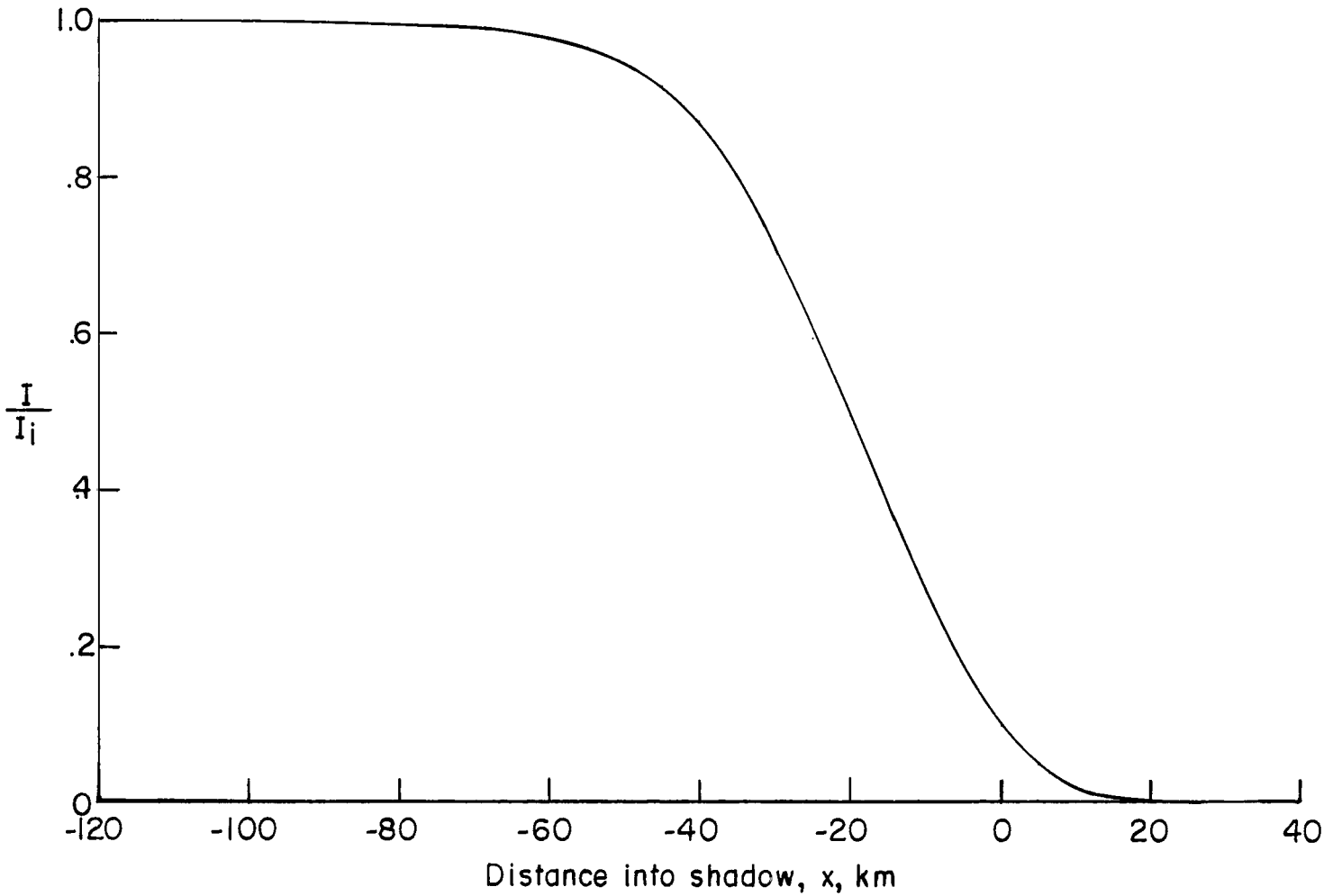

(d) Model IV; D = 8700 km.

Figure 11.- Continued.

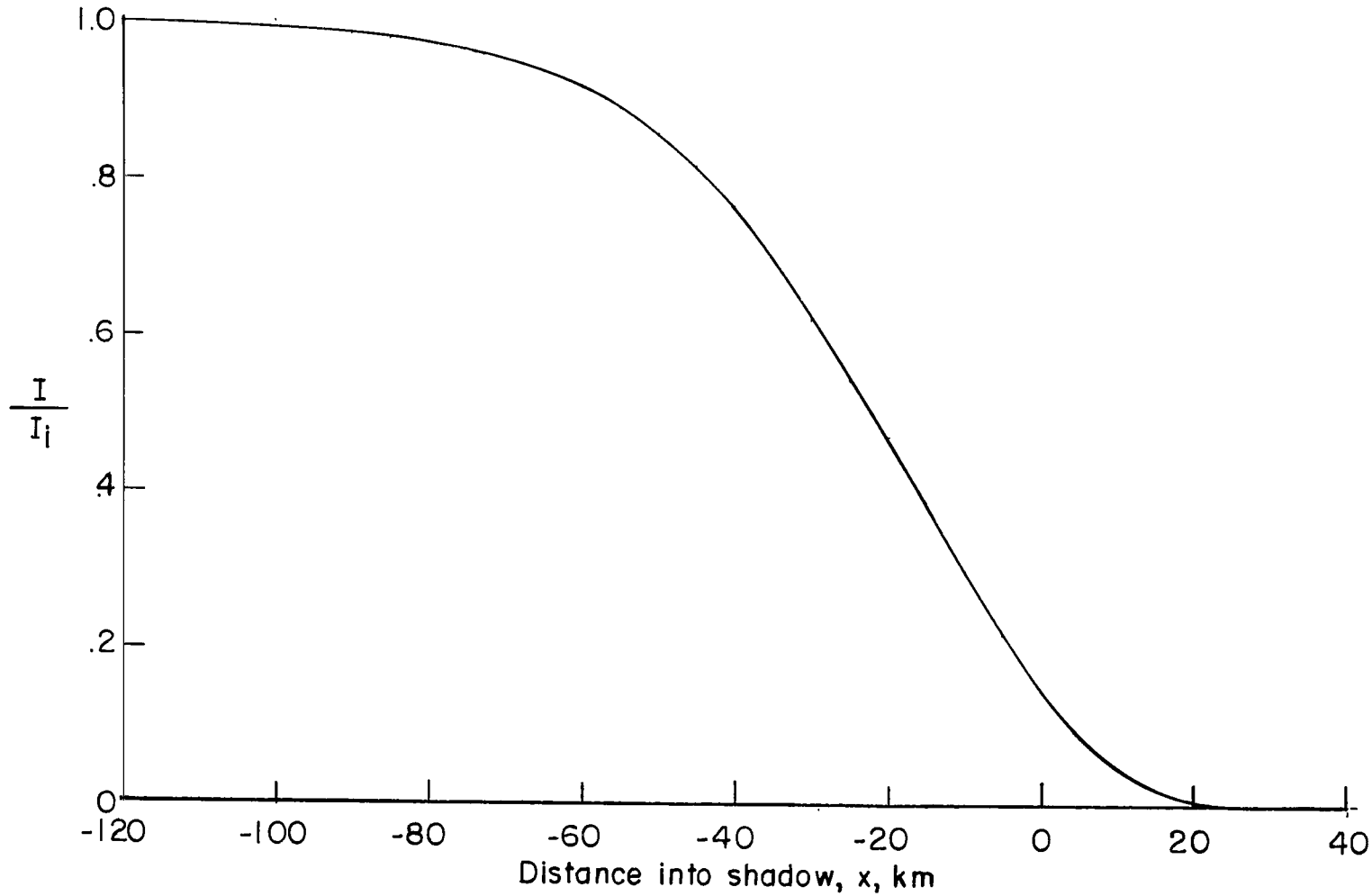

(e) Model V; D = 8700 km.

Figure 11.- Concluded.

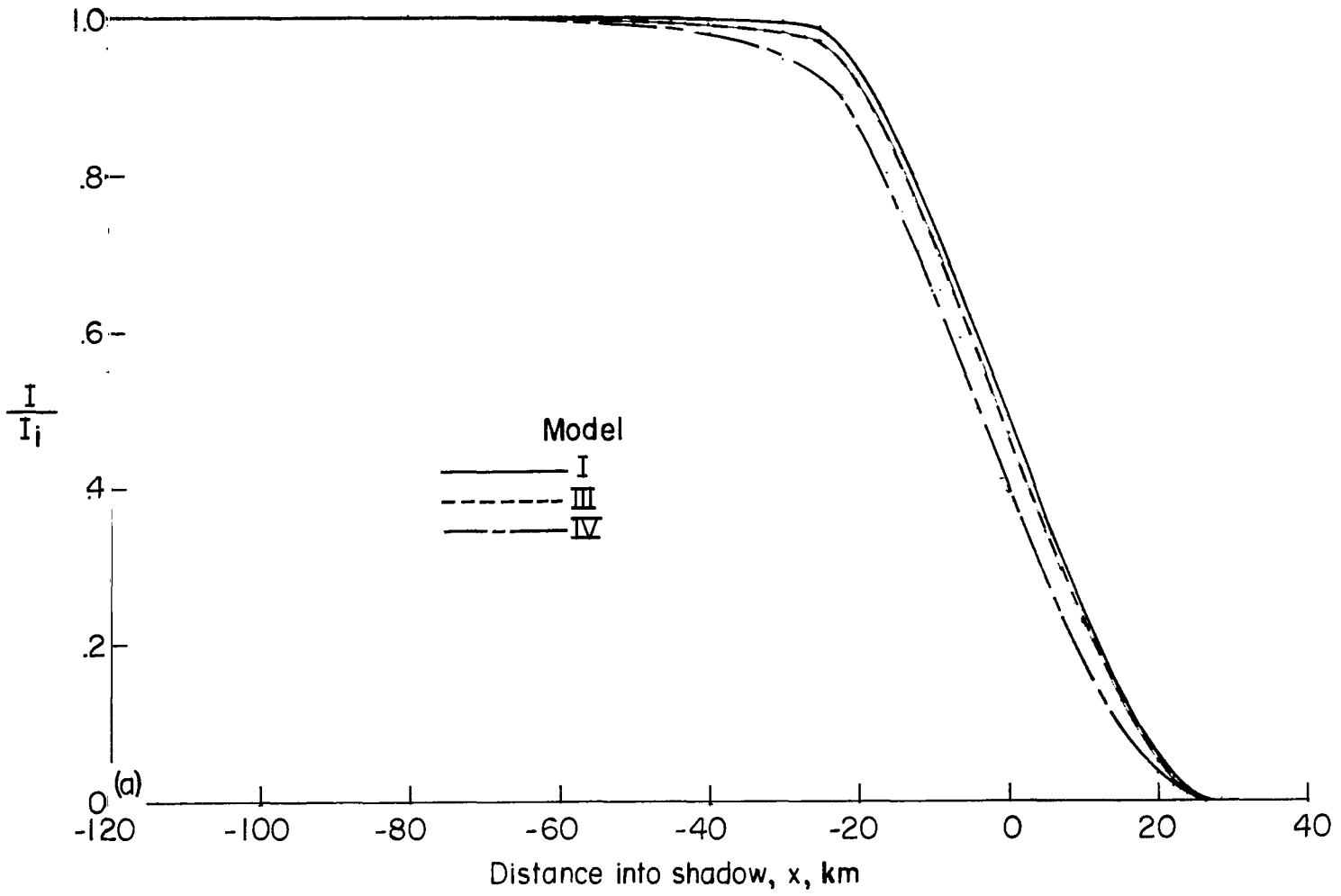

Figure 12.- Superposition of combined effects. λ = 6500 angstroms.

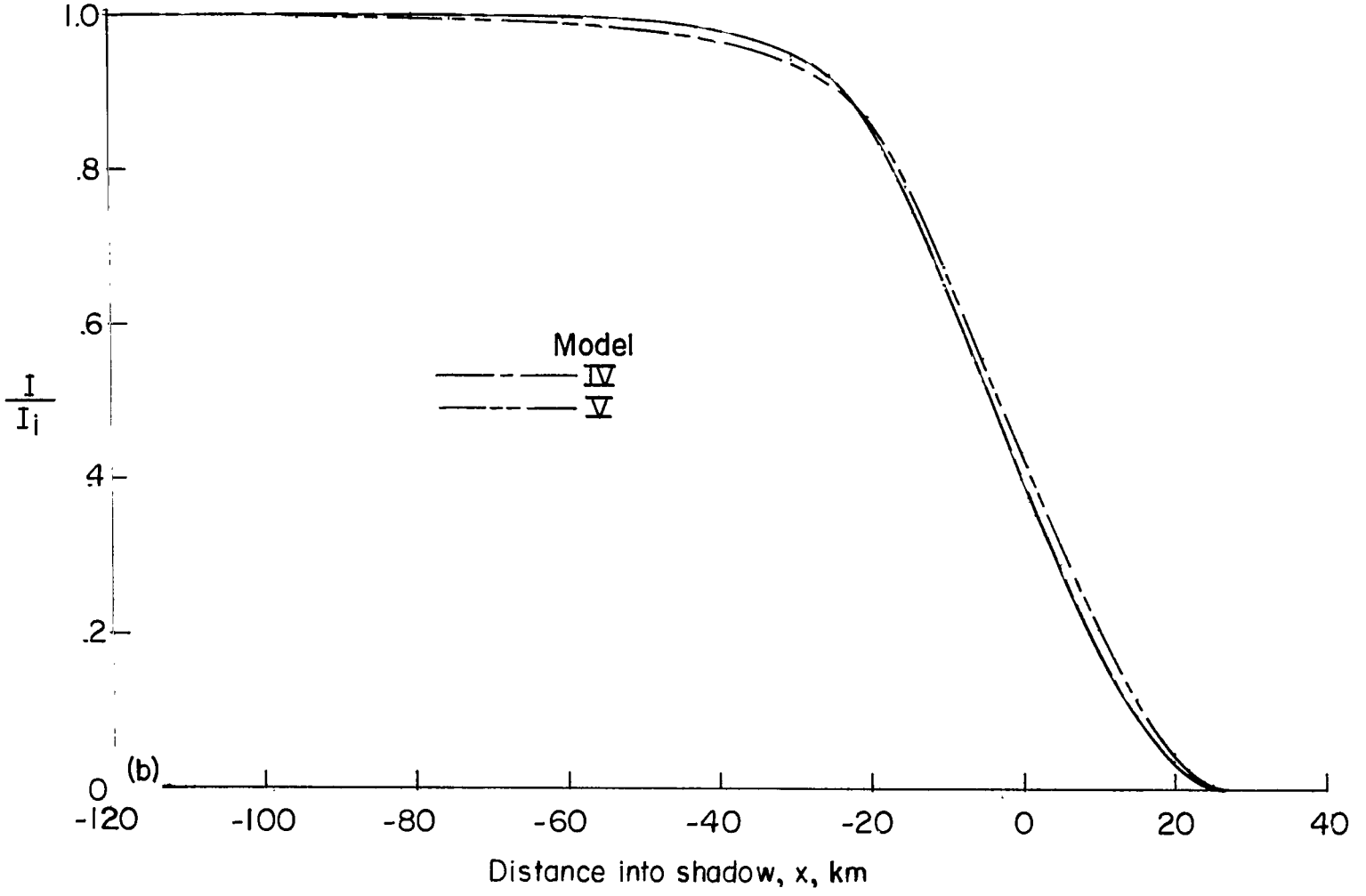

Figure 12.- Concluded.

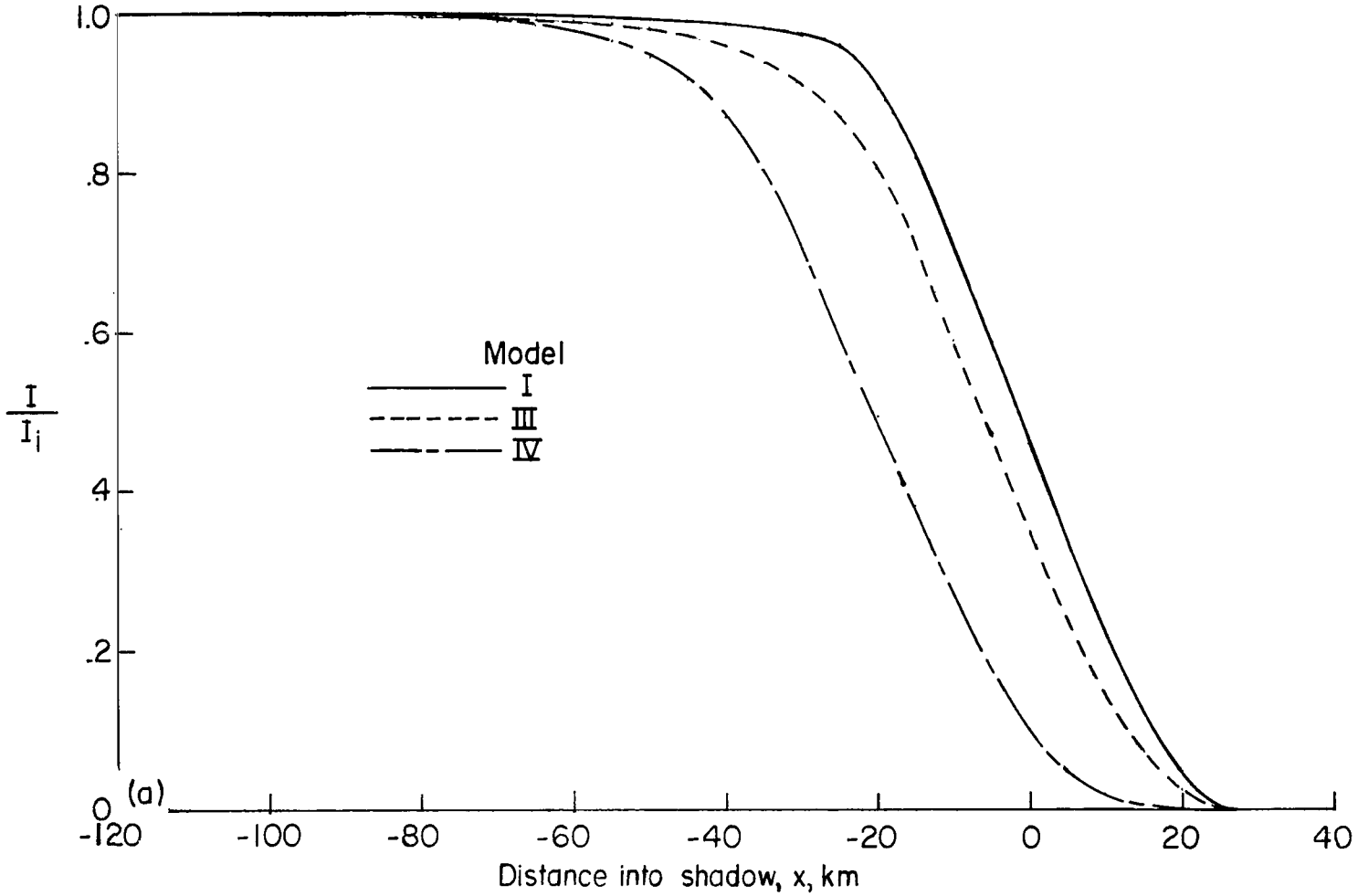

Figure 13.- Superposition of combined effects. λ = 3500 angstroms.

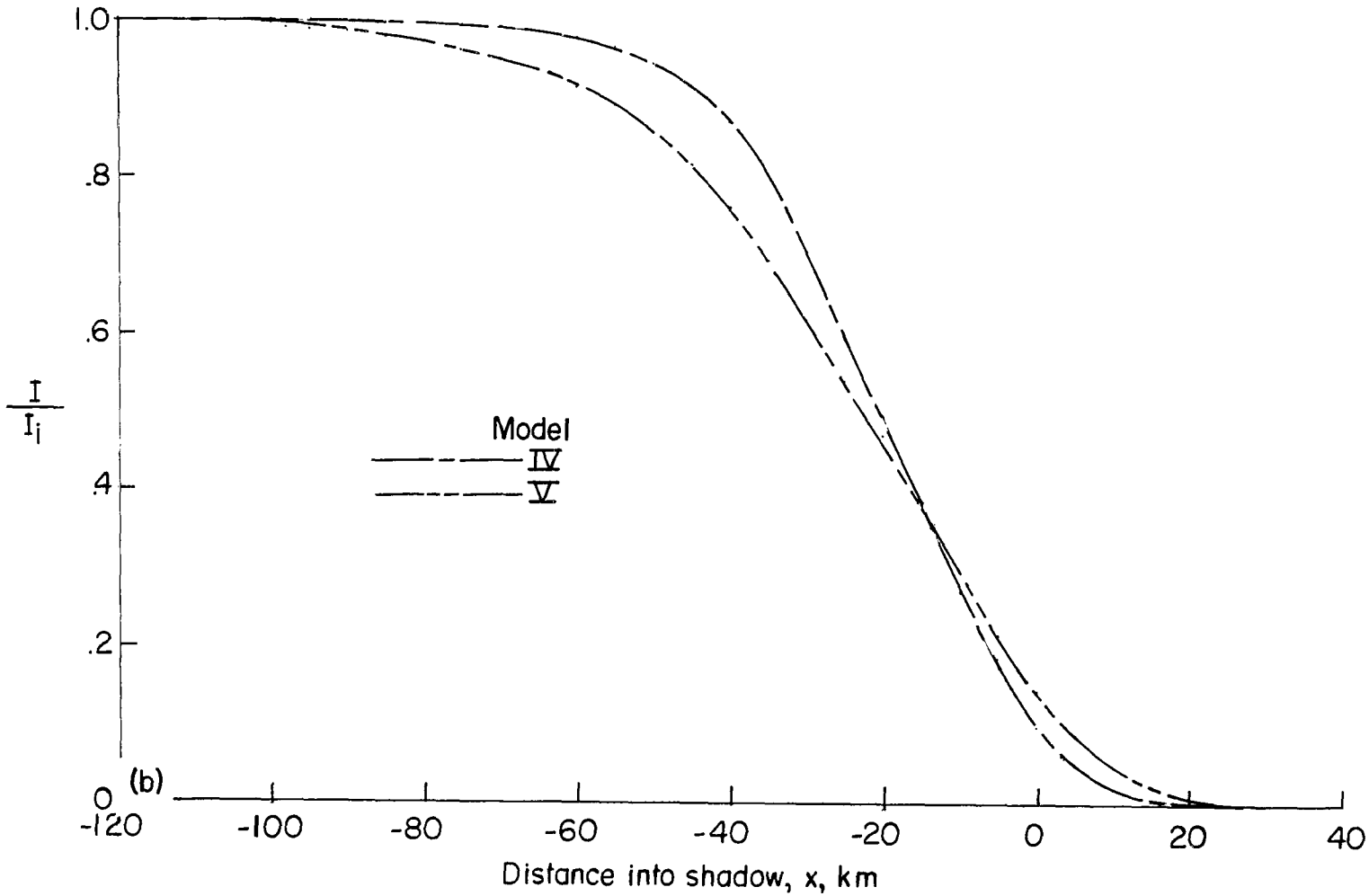

Figure 13.- Concluded.

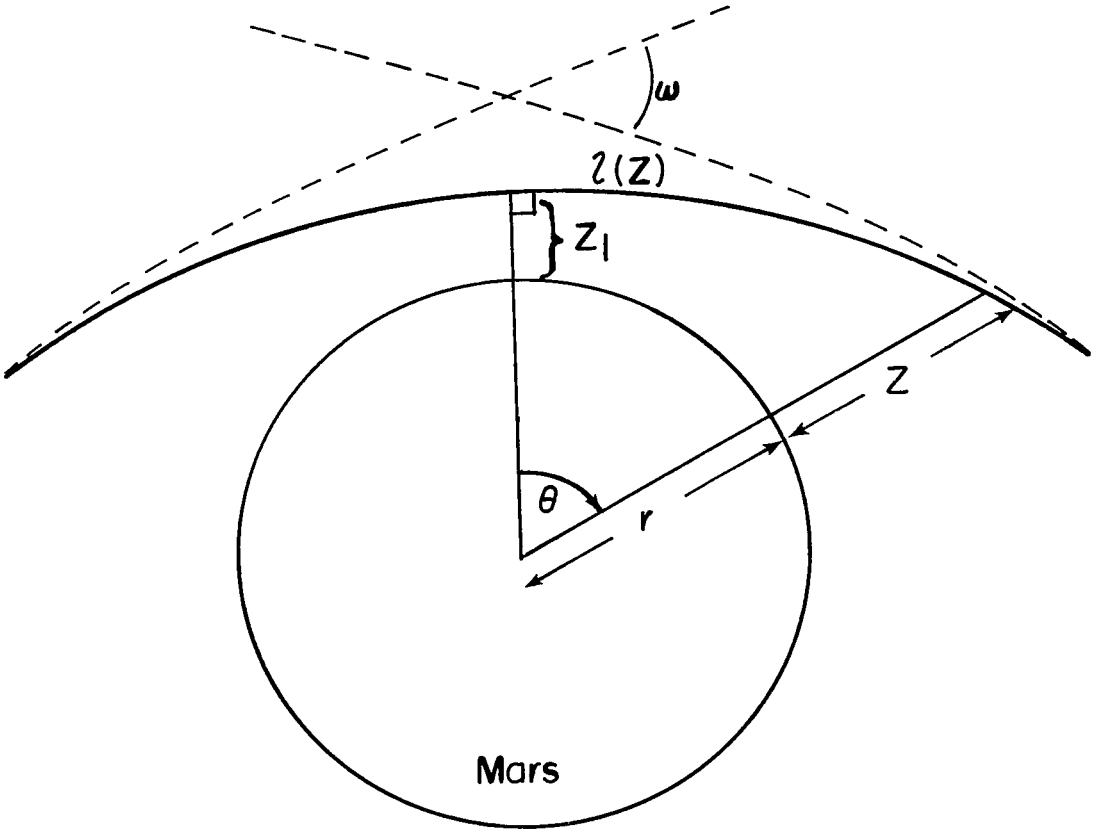

Figure 14.- Geometry for occultation.

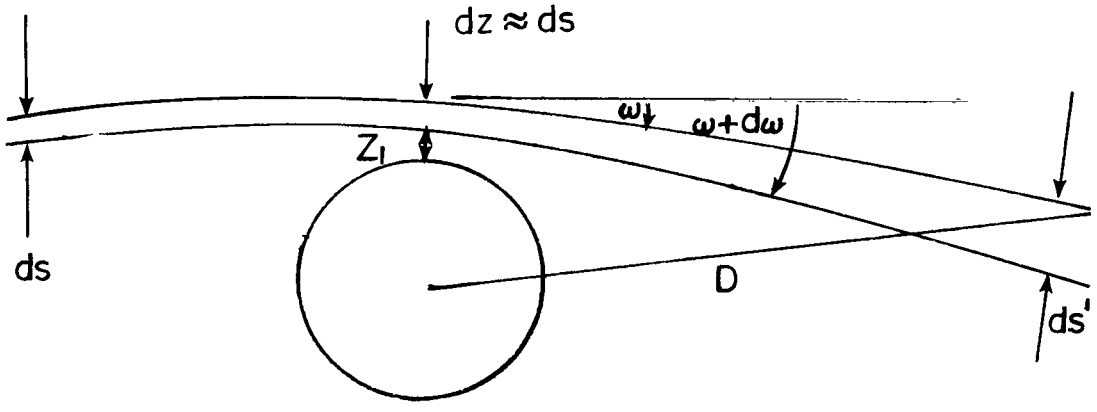

Figure 15.- The effect of differential refraction on the received intensity.

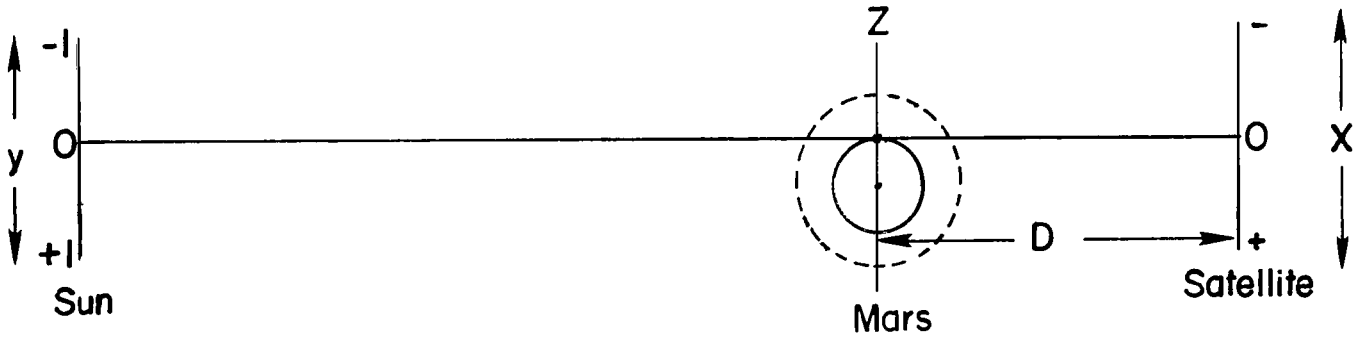

Figure 16.- Limb darkening and finite sun size effect.

"The aeronautical and space activities of the United States shall be conducted so as to contribute . . . to the expansion of human knowledge of phenomena in the atmosphere and space. The Administration shall provide for the widest practicable and appropriate dissemination of information concerning its activities and the results thereof."

—NATIONAL AERONAUTICS AND SPACE ACT OF 1958

NASA SCIENTIFIC AND TECHNICAL PUBLICATIONS

TECHNICAL REPORTS: Scientific and technical information considered important, complete, and a lasting contribution to existing knowledge.

TECHNICAL NOTES: Information less broad in scope but nevertheless of importance as a contribution to existing knowledge.

TECHNICAL MEMORANDUMS: Information receiving limited distribution because of preliminary data, security classification, or other reasons.

CONTRACTOR REPORTS: Scientific and technical information generated under a NASA contract or grant and considered an important contribution to existing knowledge.

TECHNICAL TRANSLATIONS: Information published in a foreign language considered to merit NASA distribution in English.

SPECIAL PUBLICATIONS: Information derived from or of value to NASA activities. Publications include conference proceedings, monographs, data compilations, handbooks, sourcebooks, and special bibliographies.

TECHNOLOGY UTILIZATION PUBLICATIONS: Information on technology used by NASA that may be of particular interest in commercial and other non-aerospace applications. Publications include Tech Briefs, Technology Utilization Reports and Notes, and Technology Surveys.

Details on the availability of these publications may be obtained from:

SCIENTIFIC AND TECHNICAL INFORMATION DIVISION

NATIONAL AERONAUTICS AND SPACE ADMINISTRATION

Washington, D.C. 20546